REPORT DOCUMENTATION PAGE

1a. REPORT SECURITY CLASSIFICATION	1b. RESTRICTIVE MARKINGS
Unclassified	None

2a. SECURITY CLASSIFICATION AUTHORITY	3. DISTRIBUTION/AVAILABILITY OF REPORT
	Approved for public release; distribution is unlimited.
2b. DECLASSIFICATION/DOWNGRADING SCHEDULE	

4. PERFORMING ORGANIZATION REPORT NUMBER(S)	5. MONITORING ORGANIZATION REPORT NUMBER(S)
NORDA Report 197	NORDA Report 197

6. NAME OF PERFORMING ORGANIZATION	7a. NAME OF MONITORING ORGANIZATION
Naval Ocean Research and Development Activity	Naval Ocean Research and Development Activity

6c. ADDRESS (City, State, and ZIP Code)	7b. ADDRESS (City, State, and ZIP Code)
Ocean Science Directorate Stennis Space Center, Mississippi 39529–5004	Ocean Science Directorate Stennis Space Center, Mississippi 39529–5004

8a. NAME OF FUNDING/SPONSORING ORGANIZATION	8b. OFFICE SYMBOL (If applicable)	9. PROCUREMENT INSTRUMENT IDENTIFICATION NUMBER
Office of Naval Research		

8c. ADDRESS (City, State, and ZIP Code)	10. SOURCE OF FUNDING NOS.			
800 N. Quincy St. Arlington, Virginia 22217	PROGRAM ELEMENT NO.	PROJECT NO.	TASK NO.	WORK UNIT NO.
	62759N	09552	00C	93344F
	61153N	03105	330	13338Y

11. TITLE (Include Security Classification)

Investigation of High-Frequency Acoustic Backscattering Model Parameters: Environmental Data from the Arafura Sea

12. PERSONAL AUTHOR(S)

K. Briggs, P. Fleischer, W. Jahn, R. Ray, W. Sawyer, M. Richardson

13a. TYPE OF REPORT	13b. TIME COVERED	14. DATE OF REPORT (Yr., Mo., Day)	15. PAGE COUNT
Final	From _____ To _____	February 1989	94

16. SUPPLEMENTARY NOTATION

17.	COSATI CODES		18. SUBJECT TERMS (Continue on reverse if necessary and identify by block number)
FIELD	GROUP	SUB. GR.	high-frequency acoustics, acoustic modelling, geoacoustics, photogrammetry, bottom roughness

19. ABSTRACT (Continue on reverse if necessary and identify by block number)

Bottom backscattering and geoacoustic measurements were made at a 1-km^2 site in the Arafura Sea, north of Australia. Data were collected in collaboration with the Royal Australian Navy Research Laboratory (RANRL) and the Applied Physics Laboratory-University of Washington (APL-UW) in May 1984. Sediment geoacoustic and roughness properties were characterized using box core samples, underwater video, stereo photography, and sidescan sonar imagery.

Sidescan sonar images of the bottom were relatively uniform and featureless. Sediments consisted of sand- and gravel-sized mollusk shells, shell fragments, and carbonate rocks embedded in a silt-clay matrix. Sand-gravel fractions averaged 55% and gravel fractions averaged 11% of the total sample by dry weight. Mean grain size averaged 5.3ϕ in the four cores analyzed for grain size distribution at 2-cm intervals. Compressional wave velocity ratio (125 kHz) averaged 0.989 with a coefficient of variation of 0.62%; compressional wave attenuation at the same frequency averaged 60 dB/m with a coefficient of variation of 40.4%. An average sediment porosity of 69.7% generated a density ratio of 1.49 for cores. The gravel fractions from three box cores were examined for size, weight, and volume distributions for assessing the contribution of shells to sediment volume scattering. X-radiographs were examined for three-dimensional structure and orientation of the shells. Root-mean-square height roughness was measured to be 0.368 cm for short (35.56 cm) pathlengths and 0.488 cm for longer (71.4 cm) pathlengths. Roughness power spectra from bottom height measurements had slopes near –2.2.

Model predictions of backscatter strength versus grazing angle using the measured geoacoustic and roughness properties and default values for sediment volume scattering give an underestimate of scattering strength when compared to actual data collected by APL-UW. Suggestions are made for characterizing the sediment volume scattering and bottom roughness parameters to improve the accuracy of the composite roughness model.

20. DISTRIBUTION/AVAILABILITY OF ABSTRACT	21. ABSTRACT SECURITY CLASSIFICATION
UNCLASSIFIED/UNLIMITED ☐ SAME AS RPT. ■ DTIC USERS ☐	Unclassified

22a. NAME OF RESPONSIBLE INDIVIDUAL	22b. TELEPHONE NUMBER (Include Area Code)	22c. OFFICE SYMBOL
K. Briggs	(601) 688-4690	Code 333

DD FORM 1473, 83 APR   EDITION OF 1 JAN 73 IS OBSOLETE.

Naval Ocean Research and Development Activity.

February 1989 NORDA Report 197 .

Investigation of High-Frequency Acoustic Backscattering Model Parameters: Environmental Data from the Arafura Sea

by **K. B. Briggs** and others.
P. Fleischer
W. H. Jahn
R. I. Ray
W. B. Sawyer
M. D. Richardson
Ocean Science Directorate

Foreword

Environmental acoustic support is a major effort of the Naval Ocean Research and Development Activity (NORDA) and is essential to its research emphasis on understanding the effects of the ocean environment on Navy systems and operations. Detailed acoustic and environmental data are required for developing and testing models used in the design of weapon systems. Maximizing the accuracy of these models requires incorporation of statistical variability of acoustic and environmental data collected at the ocean boundaries.

This report presents geoacoustic, bottom roughness, and volume scatterer data required to model backscattering strength from the sea floor. The environmental and acoustic data were collected on a joint NORDA/Royal Australian Navy Research Laboratory/Applied Physics Laboratory-University of Washington high-frequency acoustic experiment. The data are discussed with regard to weaknesses of existing models and with the objective of improving those models expediently. This work is part of the High-Frequency Acoustics Program (Program Element 62759N) and the Basic Research Program (61153N), and is an example of the high-quality data required to improve both the reliability of current Navy weapon systems and the understanding of ocean processes that affect naval operations.

W. B. Moseley
Technical Director

A. C. Esau, Captain, USN
Commanding Officer

Executive Summary

Bottom backscattering and geoacoustic measurements were made at a 1-km² site in the Arafura Sea, north of Australia. Data were collected in collaboration with the Royal Australian Navy Research Laboratory (RANRL) and the Applied Physics Laboratory-University of Washington (APL-UW) in May 1984. Sediment geoacoustic and roughness properties were characterized using box core samples, underwater video, stereo photography, and sidescan sonar imagery.

Sidescan sonar images of the bottom were relatively uniform and featureless. Sediments consisted of sand- and gravel-sized mollusk shells, shell fragments, and carbonate rocks embedded in a silt-clay matrix. Sand-gravel fractions averaged 55% and gravel fractions averaged 11% of the total sample by dry weight. Mean grain size averaged 5.3 ϕ in the four cores analyzed for grain size distribution at 2-cm intervals. Compressional wave velocity ratio (125 kHz) averaged 0.989 with a coefficient of variation of 0.62%; compressional wave attenuation at the same frequency averaged 60 dB/m with a coefficient of variation of 40.4%. An average sediment porosity of 69.7% generated a density ratio of 1.49 for cores. The gravel fractions from three box cores were examined for size, weight, and volume distributions for assessing the contribution of shells to sediment volume scattering. X-radiographs were examined for three-dimensional structure and orientation of the shells. Root-mean-square height roughness was measured to be 0.368 cm for short (35.56 cm) pathlengths and 0.488 cm for longer (71.4 cm) pathlengths. Roughness power spectra from bottom height measurements had slopes near -2.2.

Model predictions of backscatter strength versus grazing angle using the measured geoacoustic and roughness properties and default values for sediment volume scattering give an underestimate of 4 dB (@ 20 kHz) of scattering strength when compared to actual data collected by APL-UW. Suggestions are made for characterizing the sediment volume scattering and bottom roughness parameters to improve the accuracy of the composite roughness model.

Acknowledgments

Contents

Investigation of High-Frequency Acoustic Backscattering Model Parameters: Environmental Data from the Arafura Sea

Introduction

The Arafura Sea bottom backscattering experiment was conducted in May 1984 aboard the Australian oceanographic research vessel HMAS *Cook* in collaboration with the Royal Australian Navy Research Laboratory (RANRL) and the Applied Physics Laboratory-University of Washington (APL-UW). The experiment was designed to test the high-frequency bottom backscatter model (Jackson et al., 1986) in a soft, muddy environment with relatively little refraction. The composite roughness model predicts that, for a mud bottom like the Arafura Sea, sediment volume scattering should dominate interface roughness scattering. Because the mechanisms responsible for sediment volume scattering are not understood, this experiment would produce valuable environmental and acoustic data that could be compared for assessing volume scattering parameters. Figure 1 is a map that shows the experiment area in relation to Australia and New Guinea, including a 144-km track over which acoustic backscatter data were collected and the 1-km² area at which detailed acoustic, geoacoustic, and bottom roughness measurements were made.

Reports that describe Arafura Sea acoustic backscattering data processed in the field and vertical incidence measurements have been published (Jackson, 1986; 1987a). Some Arafura Sea geoacoustic and roughness data have also been reported in relation to other shallow-water, high-frequency acoustic experiments (Jackson and Richardson, 1985; Richardson, 1986; Jackson, 1987b; Jackson and Briggs,
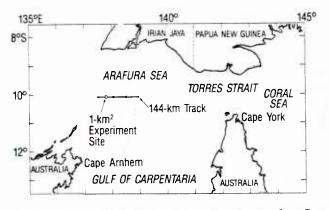
1987). This report is the first detailed account of the environmental data collected for the Arafura Sea experiment and includes a discussion of bottom roughness variability, quantifiable aspects of sediment volume scatterers in soft bottoms, and how this information may be used to improve the composite roughness model.

Materials and Methods

Site Selection

The experiment was conducted in the Arafura Sea because previous geoacoustic data from the Naval Ocean Systems Center (NOSC) showed the sediments to be of the type that would cause sediment volume scattering to dominate interface roughness scattering. The sediments are generally clayey sands and sand-silt-clays characterized by coarse calcareous material derived from relict shallow-water mollusks and coralline algae deposited during Pleistocene low sea-level periods (Jongsma, 1974). An east-west, 144-km search track was obtained prior to concentrating on a 1-km study site. The detailed experiment site was located on the Wessel Rise in the eastern portion of the Arafura Sea at approximately 10°01'S, 137°50'E.

The Arafura Sea is a shallow inland sea underlain by a sequence of sedimentary rocks over a continental crust. The seafloor is generally of low relief. Sediment input is relatively low, and the surface sediments have been subject to considerable reworking. The Arafura Sea has undergone a number of subaerial exposures during the Pleistocene, which has given its topography and sediments a mixed terrestrial/marine character (Tjia, 1966; Jongsma, 1974). The location of the study site on the Wessel Rise places it on a topographic, as well as on a deep-seated structural high (Phipps, 1967). It is therefore a site of attenuated sediment thicknesses. The relict surface sediments are the top of a Plio-Pleistocene sequence probably well under 75 m thick (Jongsma, 1974), perhaps only 10 m to 20 m. The underlying Tertiary, Mesozoic, and Paleozoic sediments are also believed to be relatively thin, but rest on an apparently thick sequence of Precambrian sedimentary rocks (Balke and Burt, 1976). A seismic

Figure 1. Search track and study site in the Arafura Sea.

refraction station on the Wessel Rise (Curray et al., 1977) supports this interpretation with the following model of velocity layers: 1.56 km/s, 280 m; 4.81 km/s, 1870 m; 5.69 km/s, 3250 m; 6.37 km/s, acoustic basement. This appears to correspond to a sequence of (1) low-density Cenozoic sediments, (2) Paleozoic-Mesozoic sedimentary rocks (possibly including some Precambrian), (3) Precambrian sedimentary and other rocks, and (4) crystalline continental crust.

Further detailed geologic description of the area is not possible because the search track and the study site unfortunately lie in an area which has not been subjected to any but the most generalized geologic study. An exhaustive review of the Australian literature showed that limited but definitive work has been conducted in the central and western parts of the Arafura Sea, but no significant published marine geologic or structural-stratigraphic information exists for the Wessel Rise region. In particular, Jongsma's detailed and comprehensive sedimentologic-stratigraphic investigation of the Arafura Sea stops at 136°E, about 160 km west of the study site, and projections from his study to the site are therefore tenuous.

Field Collection and Analysis

Sidescan sonar data were collected with a Klein Associates system operating at 100 kHz and 0.75° horizontal beamwidth. TVG-processed signals were recorded on analog magnetic tape, played back in the field and laboratory, and processed for slant range, altitude, and speed corrections. Sidescan data were collected at 100-m to 200-m ranges, and at vessel speeds usually between 4 kt and 6 kt. Lower speeds and shorter ranges (for higher-resolution imaging) were difficult to obtain successfully because of limitations in towcable length and ship operating speed. Constant winds of 25 kt to 30 kt, coupled with a 2-kt to 3-kt cross current, made ship operations at low speeds difficult; in addition, a constant rough sea state degraded the sidescan imagery.

A 3.5-kHz shallow subbottom profiler, mounted on the sidescan towfish, was operated concurrently with the sidescan sonar for large-scale roughness and subbottom structure. A comprehensive description of the sidescan and profiler systems, as well as operational methods, is given by Stanic et al. (1987). Navigation was provided by the HMAS *Cook*.

Sidescan and profiler data were collected along the search track and in the 1-km² study site. Approximately 75%, about 114 km, of the search track was surveyed at a 200-m range (400-m swath). The study site was surveyed with seven tracklines at a 100-m range (200-m swath); 100% coverage, with 40% overlap, could thus be obtained at the site. The strong cross current caused severe steering problems for the ship, and only because of the large overlap was sidescan coverage without significant holidays obtained. Navigation at the study site was accomplished with a RANRL-supplied Motorola Miniranger system employing two buoy-mounted reference units. Three attempts were made to survey the site. The first was successful, but was not used for the acoustic measurements because of ensuing navigation system problems. The second attempt was aborted after five tracklines due to drifting of the navigation buoys. The third attempt was successful, and was the location of the acoustic measurements. The sidescan data collected in the first two attempts appear to have been within a 4-km radius of the final site, and thus provide some general information on the seafloor character in the vicinity of the site.

Five grabs were taken with a small, modified version of a Van Veen grab sampler along the 144-km search track to obtain a visual impression of surface sediment variability. A 0.25 m² USNEL box corer was used to remotely collect relatively undisturbed sediment samples for determining sediment geoacoustic properties and distribution of sediment volume scatterers in the detailed experiment site. In addition, a series of grabs were taken in the experiment site to augment information on large-scale surface sediment variability determined from box cores. Four box cores were collected from the experiment site and subsampled with 6.1-cm (ID) cylindrical cores and 3 × 35-cm rectangular cores. The cylindrical cores were used to determine sediment physical and acoustic properties. The rectangular cores were used to make x-radiographs of 3-cm-thick vertical slabs of surface sediments for the purpose of determining the distribution and orientation of volume scatterers embedded in the top 24 cm of sediment (Briggs and Richardson, 1984). The remaining surface sediment (top 15 cm) from one box core was rinsed through a 1.00-mm screen to retain scatterers and macrobenthic animals. After the rectangular cores were x-rayed, the encased sediment was similarly sieved. Material retained on the screens was stained with rose bengal and preserved in 5% formalin buffered with sodium borate. Later in the laboratory, macrobenthic animals were sorted from the debris, which was then separated into gravel and very coarse sand-size fractions.

Sediment compressional wave velocity and attenuation were measured using a pulse technique after sediment temperature in the cores was equilibrated to laboratory temperature aboard ship. Temperature and salinity of the overlying water in the cores were determined with a YSI model 43TD temperature probe and an AO Goldberg temperature-compensated refractometer. Time delay measurements of 400- and 125-kHz continuous wave (CW) pulses were made at 1-cm increments through sediment cores and referenced to a core filled with distilled water using an Underwater Systems Model USI-103 transducer-receiver head.

Differences in time delay between distilled water and sediment samples were used to calculate sediment compressional wave velocity as described in greater detail in Briggs et al. (1986).

Sound velocity was calculated for the approximate in situ conditions at the time of the acoustic experiment (27.5°C, 34.5 ppt, 47 m), as well as the conditions set forth as standard (23°C, 35 ppt, 0 m) by Hamilton (1971). Sediment sound velocity is also expressed as the dimensionless ratio of measured sediment sound velocity divided by the sound velocity of the overlying water at the same temperature, salinity, and depth (Hamilton, 1970). This ratio is independent of sediment temperature, salinity, and depth, and can be used as an input for predictive models.

Compressional wave attenuation measurements were calculated as 20 log of the ratio of received voltage through distilled water to received voltage through sediment (Hamilton, 1972). Sediment attenuation values were extrapolated to a 1-m pathlength and expressed as dB/m. Sediment attenuation was also expressed as a sediment-specific constant (k), which is reported independent of frequency or pathlength by Hamilton (1972). Upon completion of acoustic measurements, the cores were refrigerated for subsequent laboratory analysis of sediment porosity and grain size distribution.

Stereo photographs of the sediment surface were made with two parallel Photosea 70D 70-mm underwater cameras operating in tandem with two Photosea 1500D 150 watt-sec (W/s) underwater strobes on a balanced steel frame. The distance between the 70-mm water-corrected lenses of the two cameras (camera base distance) was 22 cm, resulting in approximately 50% image overlap in the stereo pairs. A glass "reseau" plate mounted in the film magazines superimposed a precise arrangement of fiducial marks on the images. The reticle marks were used in the photogrammetric analysis later in the laboratory. The cameras and strobes were simultaneously actuated by a bottom contact switch connected to · a weighted compass vane. Stereo photographs were taken at distances of 3, 4, and 6 feet from the bottom by changing the length of wire connecting the bottom contact switch to the compass vane. A series of paired photographs were taken for each focal setting by bottom-bounce of the camera package while drifting across the experiment site. Several frames were trimmed off the film rolls and developed in the field to determine optimum photographic distance from the bottom (usually a function of water clarity) and to insure proper operation of the cameras. The 70-mm format film (Kodak Ektachrome ASA 64) was developed as continuous rolls on return from the field.

Visual observations of bottom features were made in real time with a remote underwater video camera. A Sea Bee CM-50 color video camera with an MK13AS (500 W-s) quartz-iodide lamp assembly was deployed on a Plexiglas vane from the hydrocast winch as the HMAS *Cook* drifted across the experiment area on three occasions. The camera and lamp were also deployed on the stereo camera package to aid the bottom-bounce method, as well as to gather real-time information on the sea floor.

Laboratory Analysis

Upon making port, cores were sectioned at 2-cm intervals by extruding the sediment with a plunger and slicing the exposed sediment off with a spatula. Of the three cores collected from each box core, two were subsampled for measuring sediment porosity. Porosity was determined on freshly sectioned sediments, measuring weight loss from subsamples dried in an oven at 105°C for 24 hours. From water content and an assumed average grain density of 2.65 g/cm^3, sediment porosity values were determined from tables developed by Lambert and Bennett (1972). Values of porosity reported here were not corrected for pore-water salinity (a small constant factor).

Grain-size analysis of sediment from one of the two cores measured for porosity was accomplished essentially as described by Folk (1965). Sediment samples were dispersed with sodium hexametaphosphate, then disaggregated by sonification (following removal of fragile gravel-sized shells 2 mm and larger). The disaggregated sample was wet-sieved through a 62-μm screen to separate the sand fraction from the silt-clay fraction. The dried sand and gravel fractions were fractionated into quarter-phi intervals (-4 to 4 ø) with a CE Tyler sieve shaker. The silt and clay fractions were analyzed for size distributions with a Micromeritics sedigraph and pipette as described by Briggs and Richardson (1984). In this case, the silt fraction was separated into half-phi intervals (4 to 8 ø), and the clay fraction was separated into whole-phi intervals (8 to 14 ø). Grain-size distributions were analyzed with a Hewlett-Packard (HP) 85 desktop computer and plotted with an HP7470A plotter. Data were plotted as weight percent histograms and cumulative weight percent from -4 to 14 ø. The mean grain size and standard deviation in phi units, skewness, kurtosis, and normalized kurtosis were calculated according to the graphic formulas of Folk (1965).

Measurement of bottom roughness was accomplished with the photogrammetric analysis of stereo photographs with a Seagle 90 Subsea stereocomparator (Stanic et al., 1987). Twelve pairs of stereo photographs were selected from 80 possible pairs taken at the 3-foot focal distance for analysis based on superior image clarity and frequent presence of the compass vane within the photographed area. Presence of the compass was required to determine possible directionality in roughness features. Bottom roughness was calculated as both root-mean-square

(RMS) height roughness and the roughness power spectrum for six cross-sectional lines in each stereo pair. The orientation of these lines was chosen to parallel the east-west and north-south course headings maintained by the ship when acoustic data were collected.

Relative sediment height was determined from not less than 128 equally spaced (at 0.28-cm intervals) height measurements along a 35.56-cm pathlength for all 72 cross-sectional lines. The relative orientation calculation in the photogrammetric software performed a de facto least-squares detrending operation on the digitized height data. RMS height roughness was calculated as standard deviation around the mean height. The mean RMS height roughness for each stereo pair and cross-sectional line was determined by calculating the square root of the mean variance in each case. The power spectral density function was calculated for each set of 128 points using manipulations suggested by Mr. Don Percival of APL-UW. A linear filter with a 20% cosine bell taper was applied to the raw data to eliminate leakage and suppress side lobes in the spectral domain. After a fast Fourier transform was used to compute the periodogram, the power spectrum was corrected for pre-whitening and smoothed by averaging spectra from each azimuthal direction, each stereo pair or all stereo pairs.

Samples saved for volume scatterer analysis from two x-ray cores (from box cores 18 and 20) and box core 17 were rinsed through a 2-mm sieve to wash out the preservative and separate the gravel and very coarse sand fractions. Material passing through the sieve was collected and examined for macrobenthic animals. The material retained on the sieve was dried and sieved into a maximum of 14 size fractions from -4.25 to -1.00 ∅ (19.03 to 2.00 mm). Particles smaller than 2 mm were not considered for this analysis of volume scatterers. This decision was based on the grain size frequency histograms and the upper limit on the acoustic frequency tested (45 kHz). The weight and proportions of shells and rocks in each size fraction were determined and recorded. Volume of each size fraction was determined with an air comparison pycnometer. In the case of large amounts of material, such as from the box core, aliquots of material were assayed for density (g/cm³) and volume was extrapolated from the entire weight of the size fraction. A minimum of two determinations were made on each size fraction to assure accuracy in values of scatterer volume.

Results
Sidescan Sonar Mapping and 3.5 kHz Profiles

The most significant characteristic revealed by sidescan sonar is the uniformity of the sea floor along the entire search track, as well as at the study site. The 200-m-range data of the search track show a featureless

bottom of relatively low backscatter intensity. Large-scale backscatter variations, such as result from gradational or abrupt changes in sediment type, or small- to large-scale bottom roughness (ripples, sand waves, sediment ridges, outcrops, reefs, channels) are absent. Occasional, ill-defined, large-scale, gradational, low-intensity backscatter variations do occur, and are probably caused by minor compositional changes in the sediment surface. This uniformity can be seen in the top half of Figure 2a. A sequence of grab samples collected along the search track, described in a following section, corroborates the uniform nature of the bottom. Small-scale backscatter variations, with the single exception of pockmarks (discussed later) are either absent or so faint as to be obscured by the always present sea-surface backscatter. The 100-m-range data of the study site duplicates the results of the search track at greater resolution. Again, with the exception of pockmarks, wave noise from the sea-surface obscures any subtle, small-scale features (Fig. 2b).

As expected from existing charts, the 3.5 kHz profiles show a bottom that is essentially flat, with only very low regional gradients. No large- or small-scale topographic discontinuities or other relief features were recorded. Subbottom penetration was excellent, within the limitations of the system, over most of the search track and the study site; maximum penetration was up to 25 m (1500 m/s sound velocity) (Fig. 2a). Layering is well-defined and essentially flat. Tentative correlation to the nearest shallow seismic profiles (Jongsma, 1974) indicates that the observed reflectors are part of the flat-lying Plio-Pleistocene sequence, which is probably less than 75 m thick at the study site. In fact, the strong reflector at 12 m in Figure 2a may correspond to Jongsma's S3 reflector (late Miocene/early Pliocene). No other stratigraphic features, such as channels, and no structural deformation, such as faulting, were found, although Jongsma's (1974) survey reveals that channels are common in this sequence to the west of the study area. However, some reduced penetration with occasional complete dropouts occurs over significant areas. The strongest observed dropout is shown in Figure 2a. Although gassy sediment may be the cause of this dropout, it is more likely (based on core samples) that variations in shell or gravel content are responsible for this dropout and for reduced penetration in other areas.

Pockmarks are a common, sporadically occurring feature along the search track. They also occur along the outer part of the study site. They are readily identified on sonographs as crater-like pits by their shadowed centers and illuminated backwalls (Fig. 2b). Sizes range to an upper limit of around 10 m. A lower size limit is not evident; 1-m pockmarks are identifiable, and the absence of smaller ones is governed in this case by operational conditions and system resolution. Depth of the pockmarks is difficult to determine due to their relatively small size on the sonographs, but the strong

4

100kHz   SONOGRAPH

uncorrected, swath width, 200m

ARAFURA SEA

3.5kHz PROFILE

full scale, 50m
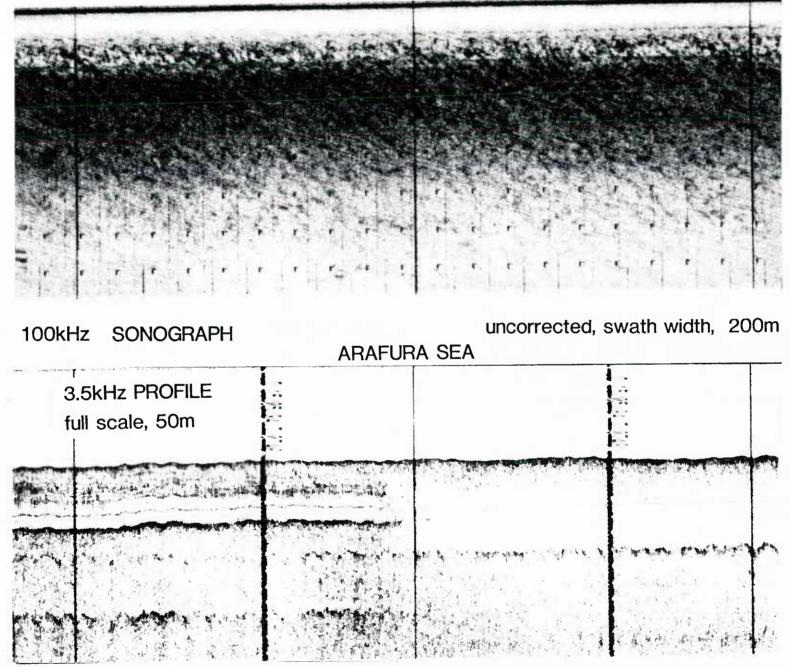
Figure 2a. Top half: One-half of a 400-m sidescan sonar swath along the search track, illustrating the uniform nature of the bottom in the Arafura Sea. Small-scale variability is backscatter from sea surface waves; this backscatter almost obscures the sediment-water interface near the top of the sonograph. Bottom half: Subbottom profile along the search track. Reflectors to almost 15 m (1500 m/s sound velocity) on left; unusually strong dropout on right. Continuous reflector in center and reflectors below it comprise a sea-surface multiple. The continuous reflector shows seafloor relief at about 4x vertical exaggeration and is unaffected by towfish altitude fluctuations.

ARAFURA SEA

100kHz SONOGRAPH   orthorectified, swath width, 100m/channel

Figure 2b. Sonograph, 200-m swath, of a portion of the study site. Area is uniform except for pockmarks in lower portion. The mottled character of the image is caused by backscatter from sea surface waves.

backwall reflections and dark shadows indicate substantial depressions on the order of 1/5 of the diameter or more. They are usually equidimensional or slightly elongated, and occasionally are accompanied by faint current lineations. Their occurrence appears to be in loose clusters of 10 to 100; however, the limited sidescan coverage hampers a reliable estimate of their areal distribution. As detailed in a following section, a portion of a large, steep-walled pit was photographed with the stereo camera. The pit has a fresh, unsedimented appearance. In view of the strong currents and shallow depth at the site, the pit must be active or of recent origin. The size and character of the pit strongly indicate that it is a pockmark.

The origin of pockmarks is often obscure. They have been observed on the Scotian and Florida shelves, in the Baltic Sea, and in the Norwegian Trench (King and MacLean, 1970; Neurauter, 1979; Hovland, 1980; Whiticar, 1981). They appear to be a feature of continental margin environments and occur on a variety of bottom types. Their formation has been attributed to numerous processes, including gas seeps, spring discharge, sediment dewatering, biological activity, and anthropogenic causes. The Arafura Sea pockmarks are similar to those described in the literature, but are generally smaller—others range from 2 m to 300 m—and they do not have well-defined atoll-like rims like those on the Florida shelf (Neurauter, 1979). Several conclusions can be drawn from the evidence of the Arafura Sea pockmarks.

• From their abundance, regional occurrence, and clustering, they seem to be a product of a significant regional process.

• Their excellent definition on sidescan sonar and the fresh appearance of the photographed pit indicate that they are contemporary features or are being actively maintained.

• Their occurrence in a wide area of uniform surface sediments, as well as any lack of correlation to shallow subbottom structure, weighs against a geologic structural origin.

• No evidence of gas in the water column or of clearly gassy sediment in the subbottom was observed on the 3.5-kHz records; this result is unfavorable to a gas-seep origin.

• However, the presence of possibly extensive older sedimentary rocks under the investigation area provides a plausible source for gas seeps, particularly since the Arafura Sea is a potential petroleum province (Balke and Burt, 1976).

The cause of the Arafura Sea pockmarks remains unclear. Geologic conditions make groundwater discharge unlikely. An anthropogenic explanation, possibly World War II bomb or depth-charge craters, is also unlikely; such craters would be significantly altered by infilling after 40 years in this dynamically active environment. Another anthropogenic explanation involves the use of this area by fishing boats from several nations. Recent technology in the prawn fishery involving benthic suction devices may be responsible for the pockmarks. A dewatering process is possible, but there is no evidence of sediment deformation in the shallow subbottom structure. A biogenic origin remains the most plausible explanation at this time. It is supported by the freshness of the pockmarks, their undefined lower size limit, and their sporadic, clustered distribution. The biological agents, however, remain unidentified.
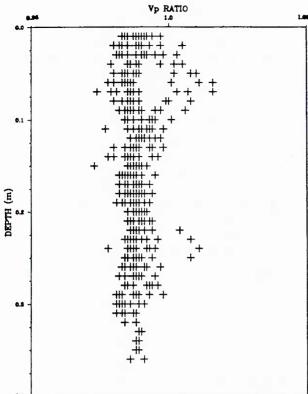
Sediment Geoacoustic Properties

Vertical distribution of sediment geoacoustic properties for the 12 cores (three from each box core) collected at the experiment site are presented in Appendix A1. Box core 20 is clearly different in character from the other three box cores. The depth interval from 2 to 10 cm in box core 20 has a higher sediment velocity ratio, higher sediment attenuation, lower porosity, and coarser mean grain size (lower phi values) than in box cores 17, 18, and 19.

Figure 3 displays the vertical distribution of sediment compressional wave velocity ratio at 125 kHz for the 12 cores. Despite the high values contributed by the 2- to 10-cm interval in cores from box core 20, the majority of the data fall around the mean velocity ratio of 0.989 and have a coefficient of variation (CV=SD×100/mean) of 0.62%. Compressional wave velocity (125 kHz) at the in situ conditions averages 1523 m/s and ranges from 1499 to 1565 m/s.

Compressional wave attenuation at 125 kHz averages 59.9 dB/m and ranges from 5.2 to 135.7 dB/m. Variability in this measurement is quite high (CV=40.38%), and values of attenuation are probably a function of scattering of the acoustic energy by shells rather than intrinsic absorption by the medium (Richardson, 1986; Briggs et al., 1986). Figure 4 displays the vertical distribution of sediment compressional wave attenuation at 125 kHz for the 12 cores.

Sediment compressional wave velocity ratio and attenuation at 400 kHz exhibit less variability than at the lower measured frequency (Fig. 5a,b). At in situ conditions, measured values of velocity at 400 kHz average 1517 m/s (velocity ratio=0.986) with a coefficient of variation of 0.37%. Measured values of attenuation at 400 kHz average 336.5 dB/m with a coefficient of variation of 34.36%. Sediment compressional wave velocity and attenuation (calculated for 23°C, 35 ppt, and 0 m depth) at 125 and 400 kHz are provided in Appendices A1 and A2, respectively.

Values of porosity range from 62.1 to 83.7% (mean=69.7%) in cores collected at the experiment site (Fig. 6). Sediments at the top 4 cm of the cores have a higher water content than deeper layers, but exhibit much greater variability. The coefficient of variation for values of porosity measured down to 35 cm is

Vp RATIO

Figure 3. Vertical distribution of sediment compressional wave velocity ratio at 125 kHz.

Vp RATIO

Figure 5a. Vertical distribution of sediment compressional wave velocity ratio at 400 kHz.

a)

ATTENUATION (dB/m)

Figure 4. Vertical distribution of sediment compressional wave attenuation at 125 kHz.
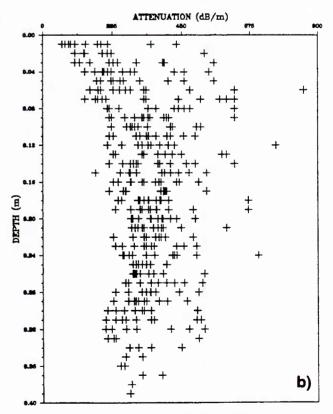
ATTENUATION (dB/m)

Figure 5b. Vertical distribution of sediment compressional wave attenuation at 400 kHz.

b)

8

POROSITY (%)
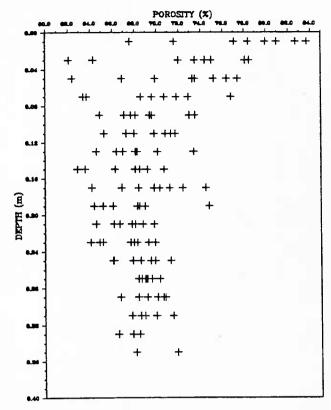
Figure 6. Vertical distribution of sediment porosity.
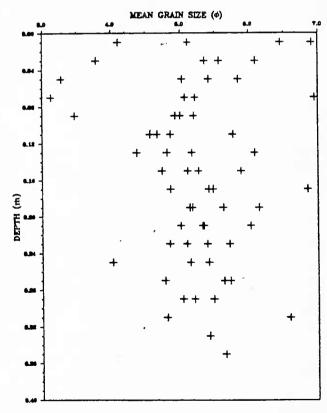

MEAN GRAIN SIZE (φ)

Figure 7. Vertical distribution of sediment mean grain size.

5.80%. The sediment bulk density calculated from the mean porosity and an assumed mean grain density of 2.68 g/cm³ (Jackson, 1986) is 1.525 g/cm³.

Sediment mean grain size ranges from 3.13 to 6.95 φ (mean=5.24 φ) in the four cores selected for grain-size analysis (Fig. 7). The mean value expressed in phi units is equivalent to a diameter of 0.026 mm. Sediments at the experiment site are extremely poorly sorted, strongly fine skewed, platykurtic clayey sands and sand-silt-clays. Hence, mean grain size is a misleading parameter due to the bimodal distribution of the sediments. Plots of weight percent-particle size frequency histograms for samples collected from box cores are displayed in Appendix B. Sediments at the experiment site are essentially sands and gravels (averaging 55% of sample weight) embedded in a silty clay matrix. (We use the term "gravel" not as the commonly used descriptive term for small rocks, but as the conventional term denoting size in the Wentworth particle size classification--particles larger than 2 mm in diameter.) Variation in mean grain size within the site is due to differences in proportions of coarser components (CV=14.86%). Coarse material consists of sand- and gravel-sized mollusk shells, shell fragments, and carbonate rocks. Sediments from box core 20 have the largest proportion of gravel and sand, especially in the top 10 cm. Table 1 shows the distribution of gravel-sized material, expressed as percentage of total sample weight, with depth in the sediment. Percentages of gravel in the four cores analyzed for grain size distributions averaged 11%.

Four grab samples collected within the experiment site suggest the box core samples are representative of the entire study area. Results of grain size analysis of the grab samples in Table 2 show a mean grain size of 6.54 φ with a coefficient of variation of 18.17%. Weight percentages of gravel from the grab samples average 9.47%. In comparison, the mean grain size and percent gravel of the top 2 cm from sediment cores averaged 5.63 φ and 8.25%, respectively.

Bottom Roughness

Impressions from video and photographic observations of the experiment site are that the sea floor is isotropically flat, but punctuated by numerous small mounds and burrows and by rare large pockmarks. The mounds are generated by burrowing infauna and are loosely aggregated features of high porosity, but are probably poor scatterers of high-frequency sound despite attaining heights of up to 10 cm. The large pockmarks are of an uncertain origin and are sparsely distributed, as described previously by sidescan sonar images. The pockmark shown in Figure 8 has relatively steep sides

9

Table 1. Weight percentages of gravel at 2-cm intervals in the four cores analyzed for grain size distribution from the experiment site.

Depth Interval (cm)	Box Core 17	Box Core 18	Box Core 19	Box Core 20
0 - 2	8.88	4.12	2.47	17.51
2 - 4	6.90	5.92	4.64	17.86
4 - 6	6.45	3.80	12.65	19.29
6 - 8	13.32	3.52	10.71	20.88
8 - 10	15.69	14.48	13.90	23.40
10 - 12	8.06	17.12	19.40	9.71
12 - 14	8.78	19.05	9.78	12.42
14 - 16	12.28	11.26	7.43	16.11
16 - 18	7.90	6.87	16.07	7.43
18 - 20	5.70	10.26	12.61	10.32
20 - 22	6.96	9.27	11.15	7.80
22 - 24	16.09	8.44	6.05	11.81
24 - 26	8.38	10.78	8.43	23.25
26 - 28	8.65	13.01	5.93	7.60
28 - 30	13.05	10.17	11.09	15.69
30 - 32		5.20	16.70	17.69
32 - 34		9.64		14.90
34 - 36		13.14		
36 - 38		8.14		

Table 2. Grain-size parameters calculated for four grab samples of surface sediments collected within the experiment site.

Parameter	Grab 9	Grab 12	Grab 13	Grab 14
Mean Grain Diameter (phi)	8.08	6.66	5.22	6.21
Standard Deviation (phi)	5.11	5.75	5.95	5.29
Skewness	-0.48	-0.13	0.20	0.15
Kurtosis	0.62	0.67	0.68	0.63
Norm. Kurtosis	0.38	0.40	0.40	0.38

and is characterized by the presence of exposed mollusk shells in and around the depression. This pit was measured photogrammetrically to have a steep side with a slope of 24° from the horizontal. At the bottom edge of the photograph the pit has a depth of 21 cm, but the pit is obviously deeper. Despite the evidence of the pits as potential scatterers of high-frequency sound, the rarity of the features precludes consideration as significant scattering sources.

The sea floor is biologically active as seen from the video images. There are numerous sessile, soft-bodied organisms on the sediment surface. Most are probably macrophytic green and red algae; some soft corals (gorgonaceans and pennatulaceans), stalked sponges, stoloniferous bryozoa, and anemones (actiniarians and ceriantharians) are visible. Figure 9 shows examples of a small mound (upper right) and burrow holes (center) in addition to a soft coral pennatulacean (lower center). The significance of these benthic flora and fauna to sound scattering is more likely to be the material to which these organisms are attached rather than the size or shape of the soft-bodied organisms themselves. Algae, bryozoa, and soft corals in particular need a hard substrate to attach the holdfasts: gravel-sized carbonate shells and rocks near the sediment surface are the only reasonable possibilities. A comparison of video and photographic images with grain-size analysis from box cores presented previously reveals relict mollusk shells

and carbonate rocks to be more numerous in the area than live macrobenthic organisms.

The values of RMS height roughness measured in the first 12 selected stereo photographs are displayed for each cross-sectional line in Table 3. Cross-sectional lines labeled A-C are oriented north-south; lines labeled D-F are oriented east-west. Values of RMS height roughness range from 0.130 to 0.730 cm with a mean value of 0.368 cm. The coefficient of variation for the RMS height roughness values is 45.72%, which is lower than coefficients for roughness data from Charleston (51.86%) and Quinault Range (72.91%) experiments (Briggs et al., 1986; Richardson et al., 1986). A t-test of means of north-south and east-west oriented roughness values shows no significant differences between the two orientations. Thus, stereo photographs confirm visual impressions of isotropic roughness at the experiment site. Plots of individual cross-sectional lines are displayed in Appendix C1.

Due to the proximity of the photographic cameras to the bottom, the maximum pathlength over which relative sediment height measurements could be made consistently is only 35.56 cm. This pathlength is longer than those used in previous analyses of experiment sites (31.5 cm) but is shorter than the optimum range of 50-100 cm (Richardson et al., 1986; Briggs et al., 1986). In order to examine bottom roughness at longer pathlengths,

Table 3. Values of RMS height roughness (35.56-cm pathlength) for 12 selected stereo photographs from the Arafura Sea experiment site. Means are calculated as the square root of the mean variance. Cross-sectional line A-C are oriented N-S; lines D-F are E-W.

| Stereo Photograph	Cross-sectional Lines						
	A	B	C	D	E	F	Mean
2-3	0.552	0.627	0.642	0.318	0.646	0.728	0.600
2-4	0.228	0.340	0.724	0.137	0.451	0.147	0.395
2-5	0.335	0.178	0.143	0.282	0.416	0.130	0.269
2-19	0.215	0.267	0.211	0.327	0.234	0.322	0.267
2-29	0.291	0.360	0.281	0.248	0.209	0.389	0.303
2-30	0.404	0.182	0.265	0.221	0.223	0.274	0.271
2-32	0.264	0.424	0.645	0.250	0.342	0.551	0.438
2-42	0.253	0.283	0.453	0.378	0.321	0.382	0.351
2-43	0.349	0.215	0.196	0.320	0.354	0.219	0.283
2-47	0.270	0.204	0.575	0.461	0.730	0.279	0.460
2-63	0.177	0.367	0.443	0.515	0.277	0.162	0.349
2-67	0.139	0.240	0.397	0.363	0.165	0.230	0.273
Mean	0.309	0.331	0.456	0.333	0.400	0.360	0.368
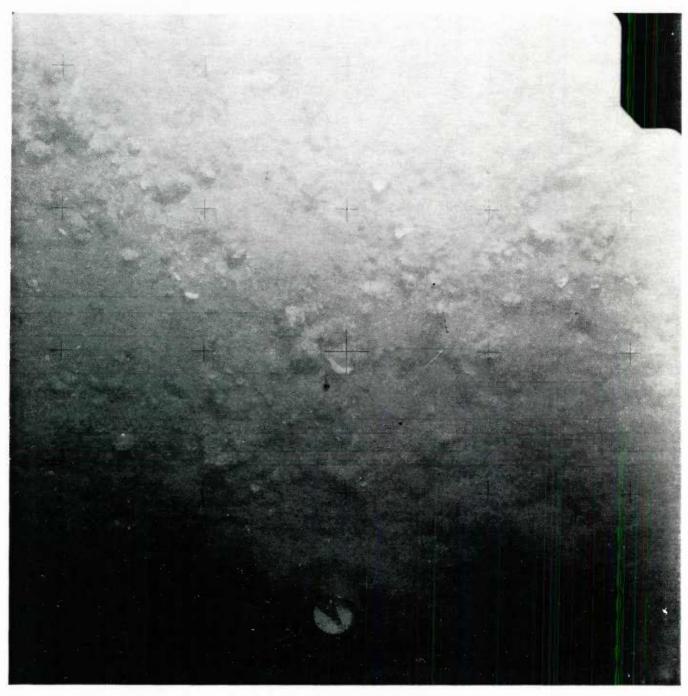
Figure 8. One half of a stereo pair taken at the edge of a pockmark. Pockmarks such as this are large but rare features of the experiment site. Note abundance of shells in and around depression.

Figure 9. One half of a stereo pair showing biogenic roughness. Note presence of soft coral (pennatulacean) in center of photo.

an additional 14 pairs of stereo photographs taken at the 4-foot focal distance were selected from 56 possible pairs for analysis based on image clarity and presence of representative features. Microtopographical features in photographs taken at the 6-foot focal distance are too indistinct to allow measurement of longer pathlengths. From these 14 pairs, 15 cross-sectional lines of 71.4 cm length are analyzed regardless of orientation (since there is no anisotropy in roughness measured from the previous 12 photograph pairs). In order to preserve the spectral resolution obtained in the original 12 photographic pairs, the digitizing interval remains at 0.28 cm. Consequently, 256 equally spaced height measurements are obtained from a 71.4-cm pathlength. Table 4 displays values of RMS height roughness for the 14 selected stereo photographs taken at the 4-foot focal length. Roughness values range from 0.188 cm to 0.792 cm with a mean value of 0.488 cm. The coefficient of variation for the roughness values at the longer pathlength is 35.64%. Cross-sectional lines for the longer pathlength are displayed in Appendix C2.

Roughness periodograms generated from digitized height data of the 35.56-cm pathlength are averaged over all 72 power spectra and plotted as dB-cm versus frequency (cm⁻¹) in Figure 10. Plots of periodograms averaged over the six power spectra corresponding to each stereo photograph are compiled in Appendix D1. The 95% confidence interval displayed on the plots is computed from tabulated chi-square values at 0.975 and 0.025 levels, with 129.03 and 10.75 degrees of freedom for Figure 9 and Appendix D1, respectively. Degrees of freedom are calculated by dividing $2 \times$ number of averaged periodograms by an adjustment factor of 1.116 to account for the effects of tapering the data (Bloomfield, 1976). The confidence interval is applicable to each point of the periodograms because bandwidth is equal to the frequency interval. All values of the periodograms fall within the 95% confidence intervals regardless of photograph or orientation. Power spectra show few differences, and these differences are most pronounced at the low frequency end of the spectra.

Slopes of roughness power spectra are more easily compared statistically. Linear regressions of (log) power on (log) frequency for each of the original 12 stereo photographs are used to generate the values of slope and intercept displayed in Table 5. Slope values varied from -1.83 to -2.54 with a mean value of -2.18. The mean value reported in the table is the slope of the periodogram that has been averaged over the 12 photographs rather than an arithmetic average of the 12 slopes. No significant differences between power spectrum slopes of north-south and east-west oriented lines exist when the equality of slopes is statistically tested by an analysis of covariance (Sokal and Rohlf, 1969). Plots of the power spectra from the two orientations are displayed in Appendix D1. Lines labeled ABC are oriented north-

south; lines labeled DEF are oriented east-west. The calculated F-statistic is 2.11 for 768 observations (64 periodogram points × 12 photographs) per orientation. The bottom roughness at the experiment site is, therefore, isotropic with respect to both relative sediment height and spatial periodicity.

The roughness periodogram generated from the 256 points of the 71.4-cm-long path and averaged over all 15 power spectra is depicted in Figure 11. Periodograms of individual power spectra from each stereo photograph taken at the 4-foot focal length are displayed in Appendix D2. Despite a higher resolution due to a smaller increment between frequency bins, the roughness periodogram representing pathlengths twice as long appears similar to the roughness periodogram in Figure 10. Another difference in the appearance of the spectrum obtained from the longer pathlength is due to the fact that the spectrum in Figure 11 is smoothed by averaging only 15 individual spectra, whereas Figure 10 represents a smoother spectrum averaged from 72 individual spectra. Table 6 displays values of slope and intercept of regression lines from power spectra of roughness measurements with a 71.4-cm pathlength. The slope of the periodogram averaged over all 15 power spectra is -2.25.

Table 4. Values of RMS height roughness (71.4-cm pathlength) for 14 selected stereo photographs (15 total cross-sectional lines) from the Arafura Sea experiment site. Mean is calculated as the square root of the mean variance. Asterisk (*) denotes new cross-sectional line from same stereo photograph. Orientations of lines are random.

Stereo Photograph	RMS (cm)
1-10	0.391
1-16	0.268
1-21	0.276
1-30	0.432
1-33	0.650
1-37	0.532
1-39	0.368
1-43	0.585
1-43*	0.506
1-44	0.574
1-45	0.792
1-49	0.512
1-50	0.548
1-54	0.188
1-55	0.295
Mean	0.488

14

Table 5. Values of power spectrum slope and intercept (cm³) for 12 selected stereo photographs (35.56-cm pathlength) from the Arafura Sea experiment site.

Photograph	Slope	Intercept (×10⁻⁴)
2-3	-2.39	3.8
2-4	-2.54	1.6
2-5	-2.43	1.8
2-19	-2.17	5.2
2-29	-2.35	3.5
2-30	-2.37	3.6
2-32	-2.29	14.2
2-42	-1.87	19.0
2-43	-1.83	12.6
2-47	-2.15	4.7
2-63	-2.15	3.9
2-67	-2.31	2.8
Mean	-2.18	6.9

Table 6. Values of power spectrum slope and intercept (cm³) for 15 selected stereo photographs (71.4-cm pathlength) from the Arafura Sea experiment site.

Photograph	Slope	Intercept (×10⁻⁴)
1-10	-2.65	2.0
1-16	-2.09	3.5
1-21	-2.19	1.8
1-30	-2.19	1.5
1-33	-2.71	1.9
1-37	-2.06	3.0
1-39	-2.00	5.0
1-43	-2.66	1.9
1-43*	-2.56	2.1
1-44	-2.16	1.6
1-45	-2.15	2.8
1-49	-1.86	5.6
1-50	-2.02	4.8
1-54	-1.92	2.4
1-55	-2.44	1.7
Mean	-2.25	4.7

Volume Scatterer Measurements

Potential sediment volume scatterers from x-ray cores and box core 17 are predominantly mollusk shell fragments. Significant numbers of pebbles and granules also are found among the gravel-sized particles. Table 7 displays the data from individual size fractions of the top 15 cm of box core 17, the 28-cm-deep x-radiograph core from box core 18, and the 23-cm-deep x-radiograph core from box core 20. Large amounts of material in the smaller-sized fractions necessitated estimating the number of particles by counting proportions on a grid. In those cases where numbers are estimated, the proportion of pebbles (granules) in the size fraction is not determined. In the size range from 2.83 to 13.4 mm, the number of shells and shell fragments is approximately equal to the number of pebbles in all three samples. The trend, however, is for the proportion of pebbles to decline in the smaller-sized fractions. The density of the scatterers ranges from 2.60 to 2.78 g/cm³ with a mean value of 2.74 g/cm³. This value is reasonable for the specific gravity of skeletal material from marine organisms, which is predominantly calcium carbonate. Scatterers less than 9.5 mm in diameter are remarkably consistent within each size fraction in the weight and volume per individual particle. The weighted average for weight and volume per particle is strongly biased toward the value for the smaller-sized fractions because there are many more particles in the smaller-sized fractions.

Some of the meristic data on the scatterers presented in Table 7 are graphed as frequency histograms in Figures 12-14. Percentages of scatterers in each size interval for box core 17 is depicted in Figure 12a. The rapid decline in numbers of scatterers as the particle diameter increases (from right to left in the graph) is consistent in all three cores (Figs. 12a-14a). Volume percentages in each size interval, or the volume each size fraction contributes to the total volume of the scatterers, is depicted in Figures 12b-14b. With few exceptions, the trend of the volume of scatterers to decrease as the particle diameter increases is identical in each sample. Because the relationship between the weight and volume of the particles (i.e., density) is constant for all practical circumstances, weight percentages of scatterers are virtually identical to volume percentages and are not graphed.

Comparison of grain-size frequency histograms from cylindrical cores (Appendix B data plotted as percentages of gravel) and cores analyzed for volume scatterers (Figs. 12-14) yields somewhat similar results. Deviations in shape of histograms between the two types of cores are acceptable because grain-size analysis is performed on only a subsample from each 2-cm-depth interval. Obtaining an accurate sample of the entire range of particle sizes would be difficult in such a small aliquot. Because of the similarity in results between cylindrical cores and cores analyzed for volume scatterers, the vertical distribution of scatterers can be examined by inspection of the frequency histograms at the 2-cm-depth intervals in Appendix B. Grain-size data show a concentration of coarser particles at sediment depth intervals of 8-16 cm and 24-32 cm. The importance of
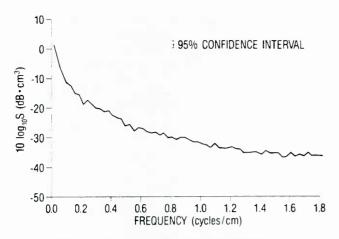
15

Figure 10. Periodogram estimate of the averaged roughness power spectrum calculated from all 72 cross-sectional lines measured from the stereo photographs taken at the 3-foot focal length.
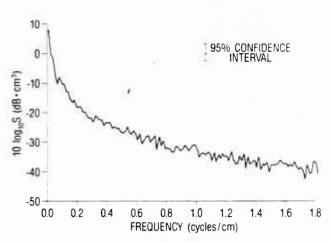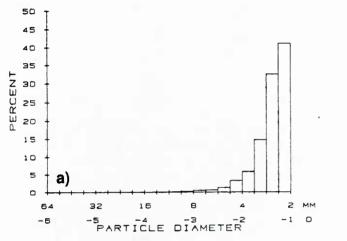
Figure 11. Periodogram estimate of the averaged roughness power spectrum calculated from all 15 cross-sectional lines measured from the stereo photographs taken at the 4-foot focal length.

Figure 12. Frequency histogram depicting (a) percentages and (b) volume percentages of gravel-size scatterers in quarter-phi interval size fractions from box core 17.
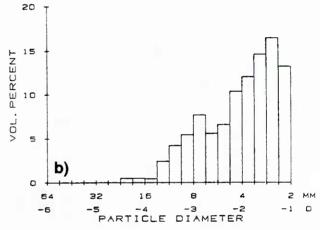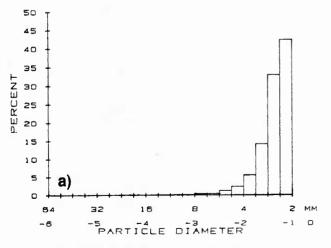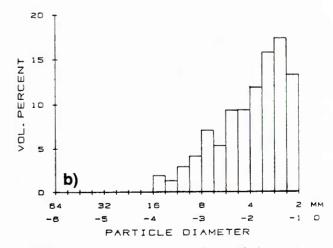

Figure 13. Frequency histogram depicting (a) percentages and (b) volume percentages of gravel-size scatterers in quarter-phi interval size fractions from x-radiograph core 18.

16

Table 7. Meristic data from quarter-phi-interval size fractions of gravel-size scatterers collected in box core 17, x-radiograph 18, and x-radiograph 20.

φ	mm	Box Core 17							x-radiograph Core 18							x-radiograph Core 20						
		Weight (g)	Volume (cm³)	Number	Propor. Pebbles	ρ (g/cm³)	Wt./Ptl. (g)	Vol./Ptl. (mm³)	Weight (g)	Volume (cm³)	Number	Propor. Pebbles	ρ (g/cm³)	Wt./Ptl. (g)	Vol./Ptl. (mm³)	Weight (g)	Volume (cm³)	Number	Propor. Pebbles	ρ (g/cm³)	Wt./Ptl. (g)	Vol./Ptl. (mm³)
-4.25	19.03	10.96	3.98	5	0	2.78	2.192	798														
-4.00	16	11.23	4.09	8	0.13	2.75	1.404	511														
-3.75	13.40	9.26	3.58	11	0	2.60	0.842	324	3.70	1.42	2	0.50	2.61	1.85	710	8.50	3.15	2	0.50	2.70	4.25	1575
-3.50	11.20	53.38	19.58	42	0.36	2.73	1.271	466	2.60	0.98	1	1.00	2.67	2.60	975	8.68	3.17	5	0.60	2.74	1.736	834
-3.25	9.50	94.87	34.16	104	0.45	2.78	0.912	328	5.95	2.19	6	0.50	2.72	0.992	365	8.76	3.23	14	0.29	2.75	0.626	231
-3.00	8	121.15	44.07	207	0.53	2.75	0.585	213	8.26	3.09	14	0.50	2.67	0.590	221	19.67	7.18	35	0.54	2.74	0.562	205
-2.75	6.70	171.73	62.81	521	0.50	2.73	0.330	121	14.58	5.32	42	0.57	2.74	0.347	127	29.95	10.92	89	0.56	2.74	0.337	123
-2.50	5.60	124.15	45.36	627	0.54	2.74	0.198	72.3	10.80	4.01	46	0.65	2.69	0.235	87.2	19.69	7.15	98	0.54	2.75	0.201	73.0
-2.25	4.75	147.24	53.61	1332*	—	2.75	0.111	40.2	19.16	7.01	137	0.61	2.73	0.140	51.2	28.58	9.72	216	0.44	2.73	0.123	45.0
-2.00	4	228.60	83.36	3488*	—	2.74	0.066	23.9	19.20	7.03	258	0.38	2.73	0.074	27.2	31.38	11.50	427	0.43	2.73	0.073	28.9
-1.75	3.36	267.19	97.17	6314*	—	2.75	0.042	15.4	24.50	8.90	608	0.35	2.75	0.040	14.6	36.71	13.34	920	0.35	2.75	0.040	14.5
-1.50	2.83	325.85	118.53	15937*	—	2.75	0.020	7.44	32.51	11.84	1582	0.28	2.75	0.021	7.58	41.93	15.24	1872	0.32	2.75	0.022	8.14
-1.25	2.38	368.55	133.62	35128*	—	2.78	0.010	3.80	35.93	13.03	3620*	—	2.76	0.010	3.60	43.80	15.90	4640*	—	2.78	0.009	3.43
-1.00	2	295.15	107.33	44451*	—	2.75	0.007	2.41	27.29	9.97	4659*	—	2.74	0.006	2.14	37.74	13.75	8648*	—	2.74	0.006	2.08
TOTAL		2229.31	811.23	108173	0.31+	2.75+	0.021+	7.50+	204.48	74.79	10955	0.53+	2.73+	0.019+	6.83+	313.39	114.25	14966	0.46+	2.74+	0.021+	7.63+

* estimated on grid

+ average

17
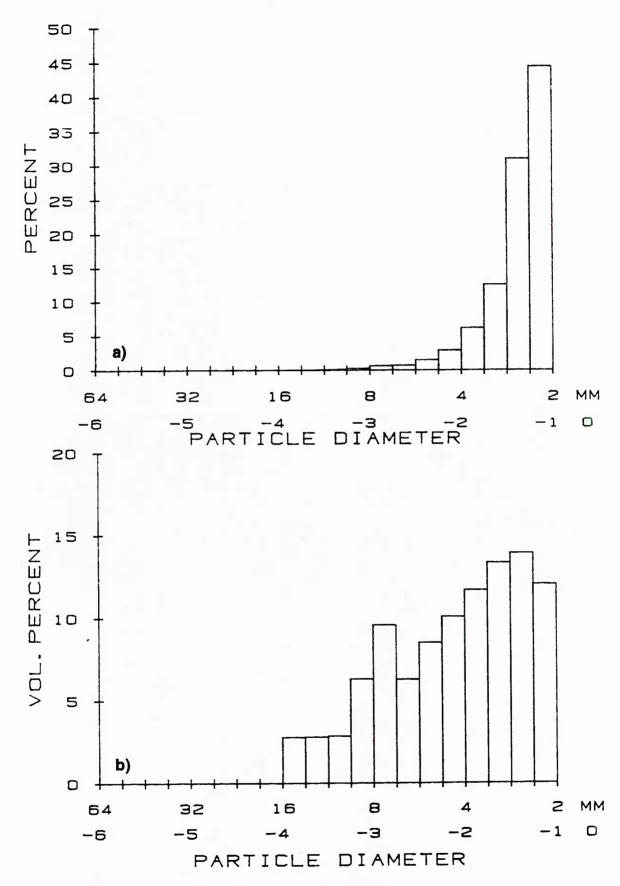
Figure 14. Frequency histogram depicting (a) percentages and (b) volume percentages of gravel-size scatterers in quarter-phi interval size fractions from x-radiograph core 20.
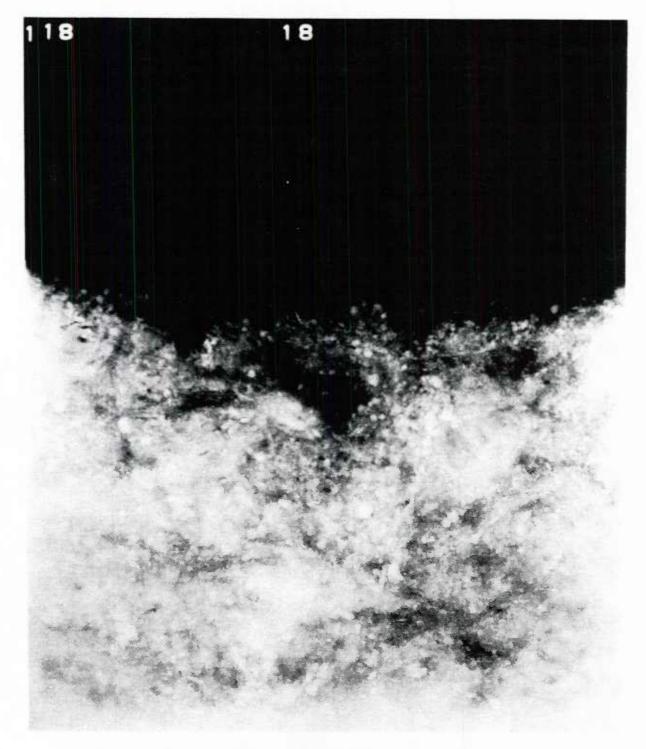
Figure 15. X-radiograph of 3-cm thick sediment slab from box core 18.

the deeper interval can not be ascertained (besides presenting resistance to further penetration of the core) because it was not sampled in its entirety in the cores analyzed for volume scatterers. Pebbles and granules are present at virtually every depth interval in the cores.

Examination of two x-radiographs collected from box cores 18 and 20 shows the inhomogeneities present within the sediment matrix (Figs. 15 and 16). The sediment-water interface is visible at the upper portion of the figures. Numerous burrows, represented by darker areas, and carbonate pebbles, represented by the whitest patches, are distributed throughout the sediment. A collapsed burrow in the center of core 20 and a subsequent filling of the void has caused the irregular appearance of the sediment-water interface in Figure 16. Mollusk shells are represented by fine white striations and a

19
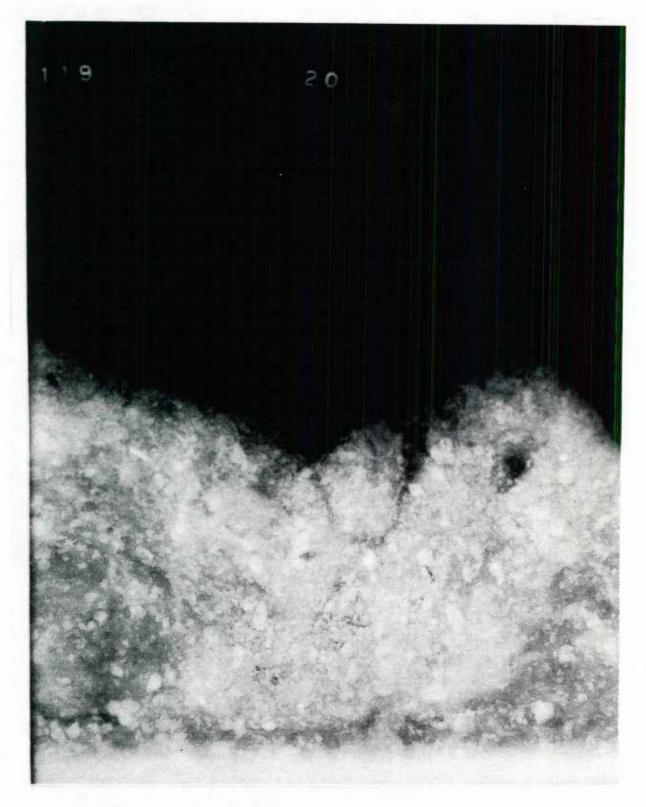
Figure 16. X-radiograph of 3-cm thick sediment slab from box core 20.

general light appearance of the x-radiograph. Some of the smaller-sized particles in the sand-sized fractions cause scattering of the x-rays and contribute to the overall light appearance of the x-radiograph. The concentration of coarse particles at 8- to 16-cm sediment depth mentioned above is evident. This shell layer appears as a lighter area between upper and lower dark areas. The beginning of the lower shell layer at 24-cm depth is evident at the bottom of Figure 15.

The orientation of scatterers within the sediment matrix is apparently random, a result of the reworking of the sediments by abundant burrowing infauna. However, presence of pebbles and granules in the top few centimeters is rare. In addition, pebbles become larger and more numerous deeper in the cores. X-radiographs produced from cylindrical cores collected from all four box cores show the same distribution pattern of shells and pebbles that appears in the two x-radiographs of the 3-cm slabs of sediment. Figures 17a and 17b are x-radiographs of cylindrical cores from which grain size analysis was conducted. These x-radiographs are the only ones made in box cores 17 and 19. The images, however, are inferior to the 3-cm slabs of sediment because of lack of constant thickness and scattering of the radiation by the cylindrical walls of the cores.

Particles that are spheroid shaped (pebbles and granules), or flat or concave/convex but are oriented with their maximum cross-sectional area exposed to the x-rays, produce the best-defined images on the film. A count of the well-defined particles on the image of x-radiograph core 18 yields only 6% of the total scatterers sieved from the core. The number of particles larger than 5 mm apparent on the film is only about a third of that particular size class collected from the core. These observations appear to cast doubt on the randomness of the orientation of the scatterers.

The failure of the majority of scatterers to produce a well-defined image on the x-ray film is due to one or more of the following: (1) orientation of many particles is such that the minimum cross-sectional area is exposed to the x-rays (scatterers perpendicular to the film plane), (2) orientation is such that particles either "shadow" upon or coalesce into other particles closer to the film, or (3) the overwhelming proportion of particles are small shell fragments that tend to be eroded and, hence, are more transparent to x-rays than the less numerous large particles. If the majority of scatterers are oriented so that the minimum area is exposed to x-rays, then the maximum area is exposed upward toward the water column or to either side. This problem is significant because the acoustic energy is incident upon the sediment volume scatterers from the upward direction. Cores collected in such a manner to produce a horizontal slab of sediment would yield information to either refute or corroborate this scenario of shell orientation. With this consideration in mind, shadowing or coalescing of scatterers become irrelevant and x-radiographs of cores collected perpendicular to the incident acoustic energy become more valuable than grain-size distributions in determining sediment volume scattering.

Despite decreased density to x-rays of smaller scatterers, the radiation that is scattered is responsible for a lighter tone of the x-radiograph, if not well-defined images of particles. Hence, determination of the lightness of tone of an x-radiograph would yield an integrated measure of the number and size of particles scattering (and to some small extent, absorbing) x-rays. A measurement of the light transmitted through the film is valuable because the film has a wide dynamic range and the measurement is less time-consuming than counting and weighing the large number of particles in each core. This consideration is worthwhile if the x-radiograph cores are of constant thickness, the exposure times to x-rays are constant, the intensity of the radiation is constant, the film is developed under identical conditions (i.e., developing time, strength of developer, and handling are constant), the light source behind the x-radiograph is constant, and the measurement is normalized to a constant area. Our x-radiographs and measurement procedure unequivocally meet these conditions. Comparison of cores from box cores 18 and 20 would be significant because of the difference in grain-size data presented previously. The average light intensity measured from x-radiograph 20 (n=17) is 1.26 times that of x-radiograph 18 (n=20). This relative measurement is accomplished with n independent, nonoverlapping determinations from each x-radiograph with an f-stop light meter and by finding the quotient of the squares of the average f-stop values of each x-radiograph image. When the actual intensity is measured more precisely in foot-candles with a light meter using the identical procedure, the results (1.32×) are in agreement, considering the variation exhibited in the x-radiograph and the failure to reproduce the measurements at the identical locations on the film.

Discussion
Prediction of Acoustic Backscattering

One important objective of the environmental data collection aspect of the experiment was to gather and analyze sufficient environmental data in order to make accurate predictions of acoustic scattering concurrent with acoustical data collection in the experiment. We also expected to refine these predictions during the experiment to help evaluate the quality of acoustic data as it was collected. The simplified model developed by Jackson (1987b) of APL-UW was used to predict high-frequency bottom backscattering from the environmental data. The version of the model used in this discussion is programmed to run on an HP85 personal computer in order to make bottom scattering predictions at sea.
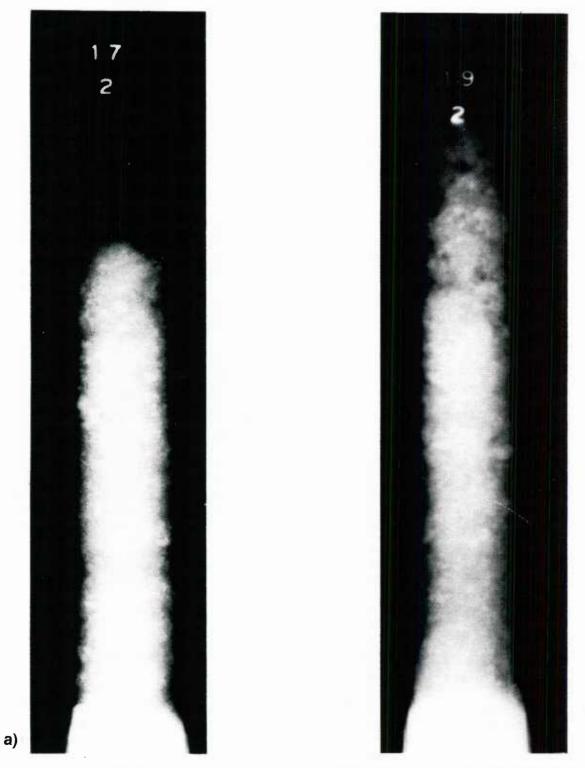
21

Figure 17. X-radiographs of 6.1-cm diameter cylindrical cores collected from (a) box core 17 and (b) box core 19.

Backscatter predictions using the APL-UW model require four environmental inputs: sediment compressional wave velocity ratio, sediment density ratio, sediment RMS roughness, and a sediment volume scattering parameter. Sediment compressional wave velocity and RMS roughness were measured directly. Sediment density ratio can be accurately calculated from porosity and the calculated bottom water density (from known bottom temperature, depth, and salinity). The sediment volume scattering parameter is the ratio of sediment volume backscattering cross section to sediment sound absorption coefficient and is estimated from compressional wave attenuation, mean grain size, or a sediment description in the APL-UW model. The sediment volume scattering contribution to backscattering strength as a function of grazing angle (θ) is mathematically expressed as

$$\sigma_v(\theta) = 1.1\sigma_2(1-r^2)^2 \sin\theta \left[1 + erf \frac{\theta - \theta_c}{\gamma_0} \right],$$

where σ_2 is the sediment volume scattering parameter, r is the Rayleigh reflection coefficient, θ_c is the critical angle, and γ_0 is an angle whose tangent is the large-scale RMS bottom slope (Jackson, 1987b). Large-scale RMS slopes are angles of only a few degrees and can be mathematically related to the RMS height roughness, h, and acoustic frequency, f, by

$$\gamma_0 = 0.354 \left(h/h_0\right)^{1.6} \left(f/f_0\right)^{0.6},$$

where h_0 is the reference length (cm) and f_0 is the reference frequency (1 kHz).

The compressional wave velocity ratio for 125 kHz at the experiment site is 0.989. This sound velocity ratio is less than unity and is characteristic of soft sediments, which show little refraction. The simplified model, however, will not accept a value for velocity ratio that is less than unity. Substituting a value of 1.001 for the velocity ratio is acceptable according to Jackson (1986). The density ratio calculated for the experiment site is 1.49. This value is an average density ratio, which incorporates all sediment porosity values from the top centimeter to 35-cm depth in the sediment. This value is probably reasonable to use because it is not known how far the acoustic energy penetrates into the sediment. RMS height roughness can be taken to be either 0.368 cm or 0.488 cm, depending on the pathlength used to determine the value. In either case, the value has to be normalized to a 100-cm pathlength for the model. Values of RMS height roughness determined at any particular pathlength are related to RMS height roughness over a 100-cm pathlength by

$$RMS_{100} = \left(100/L\right)^{0.625} \times RMS_L,$$

where RMS_L is the value of the RMS height roughness

over the measured distance L, in centimeters. The sediment-volume scattering parameter is selected to be 0.005 by Jackson (1986, 1987a,b) due to the high potential for sediment volume scattering at the experiment site.

Figure 18 shows predictions for backscattering strength (dB) at a range of grazing angles calculated for 20 kHz and using the average velocity ratio and density ratio of the experiment site sediments. The prediction calculated using the RMS height roughness determined for the 35.56-cm pathlength is slightly higher than the prediction calculated using the 71.4-cm roughness pathlength. The difference between these two predictions is noticeable only at grazing angles approaching normal incidence. The model inputs for bottom descriptors and the acoustic frequency used in each prediction are displayed in Table 8. Superimposed on the predicted curve are the actual data collected by APL-UW at 20 kHz. If we had used a value of 0.002 (the default value) for the volume scattering parameter, a 4 dB discrepancy between observed and predicted scattering strength is observed.

As depicted in Figure 18, there is no real disparity in predicted backscattering strength for different inputs of RMS height roughness obtained at the 35.56-cm and 71.4-cm pathlengths. A larger difference in roughness inputs exists between the maximum and minimum values of RMS height roughness determined at the longer pathlength (Table 8). Figure 19 shows that backscattering predictions are essentially the same (except at grazing angles approaching normal incidence and very small grazing angles) within the range of roughness values measured at the 71.4-cm pathlength.

Predictions from the simplified model using 0.005 as the volume scattering parameter compare favorably with backscattering strength data collected during the experiment (Jackson, 1986, 1987a). Although the fit
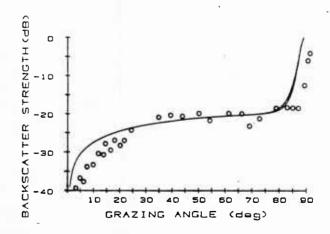

Figure 18. Predicted bottom backscatter strength (dB) versus grazing angle calculated for input values in Table 8: Differences in predictions depend on RMS height roughness determined from 35.56-cm and 71.4-cm pathlengths.

23

Table 8. Values for model inputs for each predicted curve (high and low) in each figure in the discussion section. Inputs are compressional wave velocity ratio (Vp), density ratio (ρ), RMS roughness (cm) over 100-cm pathlength (RMS_{100}), sediment volume scattering parameter (σ_2), and acoustic frequency (kHz).

Figure	Prediction	Vp	ρ	RMS$_L$	RMS$_{100}$	σ$_2$	kHz
18	high	1.001	1.49	0.368	0.702	0.005	20
	low	1.001	1.49	0.488	0.602	0.005	20
19	high	1.001	1.49	0.792	0.941	0.005	20
	low	1.001	1.49	0.188	0.232	0.005	20
20	high	1.001	1.26	0.488	0.602	0.005	20
	low	1.001	1.61	0.488	0.602	0.005	20

Figure 19. Predicted bottom backscatter strength (dB) versus grazing angle calculated for input values in Table 8: Differences in predictions depend on maximum and minimum values for RMS height roughness determined from 71.4-cm pathlengths.
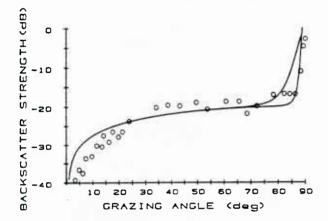

Figure 20. Predicted bottom backscatter strength (dB) versus grazing angle calculated for input values in Table 8: Differences in predictions depend on maximum values for sediment density ratio in the top centimeter of sediment.

between the model and data is satisfactory, the model predicts higher backscattering strength than observed at very small grazing angles. The discrepancy between measured and predicted results at small grazing angles is at most 4 dB (@ 10°) and is probably due to the inability of this version of the model to accept velocity ratios less than unity. Jackson (1987a) finds good agreement between measured and predicted results at large grazing angles if a very low value for density ratio is chosen for the model input. However, the value of the density ratio chosen to fit the data (1.13) would be the result of an average sediment porosity at the experiment site of 92%. Actual values of measured sediment porosity in the top 4 cm of sediment range from 62.1 to 83.7%. The density ratios corresponding to these minimum and maximum values are given in Table 8, and the backscattering strength predictions are displayed in Figure 20. The upper predicted curve using the lower bound of density ratio crosses the lower curve just beyond the 75° grazing angle to give predicted values closer to measured values at the very large grazing angles.

Values of sediment porosity greater than 83.7% would be rare, if not improbable, at the experiment site. Indeed, a situation producing a ubiquitous layer of sediment of 92% porosity (e.g., a shallow nepheloid, or benthic boundary layer) would be obvious in observations made with the video and stereo cameras. Upon review of the tape of the video surveys, the only possible source of bottom reflection loss at the sediment-water interface occurring with significant frequency is biogenic. Areas of the sediment surface are frequently covered by what appears to be mats of macrophytic calcareous algae, colonies of stoloniferous bryozoans and tubes constructed of sediment by benthic organisms. Distribution of these mats is patchy and it is not at all clear why they are not represented in the box core samples if they exist in sufficient numbers to be acoustically significant. It is also not clear whether calcareous algae would create a bottom reflection loss or be a strong source of backscattering.

The environmental data collected to describe the velocity and density contrasts between water and

24

sediment are considered to be reliable for use as model inputs. For the muddy sediments characteristic of the experiment site in the Arafura Sea, the interface roughness measurement is adequate as a model input. Although there is evidence of variability in the roughness at the experiment site due to biological activity, overall the bottom can be considered to be flat with random small-scale perturbations. The most significant property of the sediments must be the large amount of buried shell material. This shell material is most likely responsible for the need to use a high value for the sediment-volume scattering parameter. In this discussion, we have settled on a value based on the ratio of the sediment-volume backscattering cross section to the sediment absorption coefficient. However, use of the sediment compressional wave attenuation at 125 kHz to estimate the sediment absorption coefficient may be misleading. Much of the attenuation of the 125-kHz energy is due to scattering from the shells in the sediment rather than intrinsic absorption (Richardson et al., 1986; Briggs et al., 1986; Richardson, 1986). How this fact affects the volume scattering parameter is uncertain because the presence of shells affects the volume backscattering cross section, as well as the calculation of the sediment absorption. An effort to develop the sediment-volume scattering parameter from a deterministic approach would be valuable to the model.

Physical Descriptors as Model Parameters

The simplified model uses the four bottom descriptors of compressional wave velocity ratio, sediment density ratio, sediment-volume scattering parameter, and RMS height roughness to make predictions of backscattering strength. Measurements of velocity and density ratios are reliable for describing impedance differences at the sediment-water interface. The sediment-volume scattering parameter and RMS height roughness inputs are required to describe impedance differences other than interfacial and the shape of the interface surface, respectively. Measurement of these last two descriptors is less straightforward than the first two descriptors because of uncertainty in our knowledge of acoustic bottom interaction. The specific characters or features of volume scatterers and interface relief that describe the reflection characteristics of the bottom are under debate.

Meristic analysis of the volume scatterers from box core 17 and x-radiograph cores 18 and 20 (Table 7) may provide useful data for development of new model inputs or modification of the presently used input for sediment volume scattering. The volume within the sediment matrix occupied by the scatterers provides information on the undefined potential for scattering by the shells, shell fragments, and pebbles. Because each sample contained a different volume of sediment, the total volume of scatterers is divided by the calculated volume of sediment containing the scatterers. Values of 0.022, 0.025, and 0.048 for cores 17, 18, and 20 are calculated as the volume scattering coefficients, or simple descriptors of the capacity of the sediment to scatter acoustic energy from within the sediment volume. It is significant to note the difference in amount of scatterers present in core 20 compared with the other two cores: almost twice the volume of scatterers is in core 20 than in cores 17 or 18. An indication of this result appears in mean grain-size data of Figure 7 and observations of the x-radiographs of cores 18 and 20 (Figs. 15 and 16). Obviously, variation in concentration of sediment volume scatterers is a characteristic of the experiment site. Results of acoustic data analysis (Jackson, 1986), however, show practically no variability in reverberation strength at the site. Either box core 20 is an anomaly in an otherwise uniform sediment medium or differences in scatterer amounts at this dense concentration are largely irrelevant in determining scattering strength.

A similar result is obtained by performing calculations on the weight data instead of the volume data. The proportion of bulk sediment weight due to scatterers (particles larger than 2 mm, by our definition) is the total weight of the scatterers divided by the calculated weight of sediment surrounding the scatterers. Values of 0.041, 0.046, and 0.091 for cores 17, 18, and 20 are calculated as the volume scattering factors, or ratios of scatterers to sediment exclusive of scatterers. A sediment bulk density of 1.525 g/cm³ is used to calculate the mass of sediment constituted by sand-, silt-, and clay-sized particles. Because density of the material making up the scatterers is relatively constant (Table 7), a similar trend in values results (0.023, 0.026, and 0.051) from using volume data to calculate the ratio of scatterers to sediment exclusive of scatterers.

Another approach to describe the potential scattering capability of the scatterers embedded in the sediment is to determine the number, or density, of scatterers per unit volume of sediment (inclusive of scatterers). Values of 2.88, 3.73, and 6.20 per cm³ for cores 17, 18, and 20 are calculated as volume scattering densities, or concentrations of scatterers per unit volume of sediment. Again, core 20 is notable in its higher value than the other two cores. This criterion and the two previously mentioned criteria relating to total volume and weight may be useful for determining the level of volume scattering in an integrated approach. The integrated approach, however, assumes that all particles are alike in their ability to scatter acoustic energy.

Other characteristics of scatterers worth considering are the cross-sectional area and the thickness of the particles. These characteristics are inherently variable with respect to particle size and should be determined within each size class. Separation of the scatterers into quarter-phi intervals results in up to 14 size classes
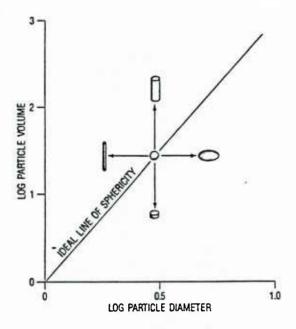
25

Figure 21. Relationship between particle volume and particle diameter and tendencies for particle shape.

Figure 22. Plot of (log) average particle volume versus (log) average particle diameter for each of the 14 size classes of gravel-size scatterers sieved from box core 17.

Figure 23. Plot of (log) average particle volume versus (log) average particle diameter for each of the 12 size classes of gravel-size scatterers sieved from x-radiograph core 18.

based on the minimum dimension of the particle. It is important to remember in developing volume scattering parameters that the scatterers are partitioned according to the narrowest diameter. Because of this fact it is difficult to derive the average thickness or maximum cross-sectional area in each size class without determining an index of shape for the scatterers. The two available measurements related to the shape of scatterers are volume and diameter. A log-log plot of particle volume as a function of particle diameter is depicted in Figure 21. The relationship between the volume and the diameter of a sphere appears as the solid line of positive slope in the plot. Deviations from the line indicate departure from sphericity; depending on the direction from the line, the shape of the particle can vary from cylindrical to discoidal (up-down) or elongate to flat (left-right). Particles that have high values for volume but small values for diameter have a longer dimension than what is used for classification (i.e., the narrowest side passed through the sieve). The scatterers in this category would be represented by points to the left of the line of sphericity. Particles that have large values for diameter but low values for volume are flattened. The scatterers in this category would be represented by points to the right of the line of sphericity.

Figures 22-24 show log-transformed values of average particle volume as a function of log-transformed average particle diameter for the three cores analyzed for volume scattering. The midpoint in each size class is used to represent the average particle diameter. In most cases the values fall to the right of the line of sphericity. In Figures 23 and 24, one value falls on the line. In the two cases noted, the size class contains either solely a pebble or a pebble much larger than a shell. The closer a data point is to the model, the greater the collective scatterer volume is influenced by the pebbles. The linear regression slopes through the data points from each core are nearly parallel to the line of sphericity (average of the three slope values is 3.01 vs. 3.00 for the ideal). Thus, the relationship between the volume and diameter of the scatterers reasonably approximates the model for spherical particles.

The distance from each data point to the line of sphericity determines the error in predicting the cross-sectional area of the scatterers in each size class from the midpoint value for particle diameter. Because the

26

Figure 24. Plot of (log) average particle volume versus (log) average particle diameter for each of the 12 size classes of gravel-size scatterers sieved from x-radiograph core 20.

data fall to the right of the model in the majority of cases, the difference in diameter represents the extent to which values of the cross-sectional area will be overestimated using the size class midpoint value for diameter. Scatterer cross-sectional area is calculated from values of size sediment volume scattering. The volume within the sediment matrix occupied by the scatterers provides information on the undefined potential for scattering by the shells, shell fragments, and pebbles. Because each sample contained a different volume of sediment, the total volume of scatterers is divided by the calculated volume of sediment containing the scatterers. Values of 0.022, 0.025, and 0.048 for cores 17, 18, and 20 are calculated as the volume scattering coefficients, or simple descriptors of the capacity of the sediment to scatter acoustic energy from within the sediment volume. It is significant to note the difference in amount of scatterers present in core 20 compared with the other two cores: almost twice the volume of scatterers is in core 20 than in cores 17 or 18. An indication of this result appears in mean grain-size data of Figure 7 and observations of the x-radiographs of cores 18 and 20 (Figs. 15 and 16). Obviously, variation in concentration of sediment volume scatterers is a characteristic of the experiment site. Results of acoustic data analysis (Jackson, 1986), however, show practically no variability in reverberation strength at the site. Either box core 20 is an anomaly in an otherwise uniform sediment medium or differences in scatterer amounts at this dense concentration are largely irrelevant in determining scattering strength.

A similar result is obtained by performing calculations on the weight data instead of the volume data. The proportion of bulk sediment weight due to scatterers (particles larger than 2 mm, by our definition) is the total weight of the scatterers divided by the

calculated weight of sediment surrounding the scatterers. Values of 0.041, 0.046, and 0.091 for cores 17, 18, and 20 are calculated as the volume scattering factors, or ratios of scatterers to sediment exclusive of scatterers. A sediment bulk density of 1.525 g/cm^3 is used to calculate the mass of sediment constituted by sand-, silt-, and clay-sized particles. Because density of the material making up the scatterers is relatively constant (Table 7), a similar trend in values results (0.023, 0.026, and 0.051) from using volume data to calculate the ratio of scatterers to sediment exclusive of scatterers.

Another approach to describe the potential scattering capability of the scatterers embedded in the sediment is to determine the number, or density, of scatterers per unit volume of sediment (inclusive of scatterers). Values of 2.88, 3.73, and 6.20 per cm^3 for cores 17, 18, and 20 are calculated as volume scattering densities, or concentrations of scatterers per unit volume of sediment. Again, core 20 is notable in its higher value than the other two cores. This criterion and the two previously mentioned criteria relating to total volume and weight may be useful for determining the level of volume scattering in an integrated approach. The integrated approach, however, assumes that all particles are alike in their ability to scatter acoustic energy.

Other characteristics of scatterers worth considering are the cross-sectional area and the thickness of the particles. These characteristics are inherently variable with respect to particle size and should be determined within each size class. Separation of the scatterers into quarter-phi intervals results in up to 14 size classes based on the minimum dimension of the particle. It is important to remember in developing volume scattering parameters that the scatterers are partitioned according to the narrowest diameter. Because of this fact it is difficult to derive the average thickness or maximum cross-sectional area in each size class without determining an index of shape for the scatterers. The two available measurements related to the shape of scatterers are volume and diameter. A log-log plot of particle volume as a function of particle diameter is depicted in Figure 21. The relationship between the volume and the diameter of a sphere appears as the solid line of positive slope in the plot. Deviations from the line indicate departure from sphericity; depending on the direction from the line, the shape of the particle can vary from cylindrical to discoidal (up-down) or elongate to flat (left-right). Particles that have high values for volume but small values for diameter have a longer dimension than what is used for classification (i.e., the narrowest side passed through the sieve). The scatterers in this category would be represented by points to the left of the line of sphericity. Particles that have large values for diameter but low values for volume are flattened. The scatterers in this category would be represented by points to the right of the line of sphericity.

27

Figures 22-24 show log-transformed values of average particle volume as a function of log-transformed average particle diameter for the three cores analyzed for volume scattering. The midpoint in each size class is used to represent the average particle diameter. In most cases the values fall to the right of the line of sphericity. In Figures 23 and 24, one value falls on the line. In the two cas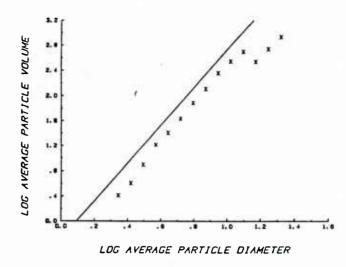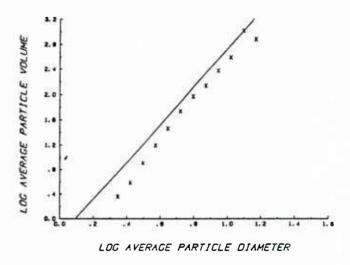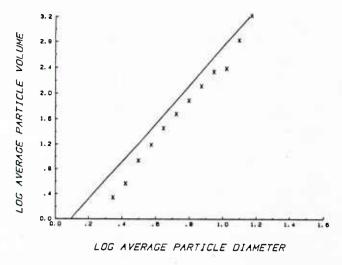es noted, the size class contains either solely a pebble or a pebble much larger than a shell. The closer a data point is to the model, the greater the collective scatterer volume is influenced by the pebbles. The linear regression slopes through the data points from each core are nearly parallel to the line of sphericity (average of the three slope values is 3.01 vs. 3.00 for the ideal). Thus, the relationship between volume and diameter of the scatterers reasonably approximates the model for spherical particles.

The distance from each data point to the line of sphericity determines the error in predicting the cross-sectional area of the scatterers in each size class from the midpoint value for particle diameter. Because the data fall to the right of the model in the majority of cases, the difference in diameter represents the extent to which values of the cross-sectional area will be overestimated using the size class midpoint value for diameter. Scatterer cross-sectional area is calculated from values of size class midpoint diameter and measured average volume, displayed in Table 9 with the respective total (maximum) calculated cross-sectional areas. The greatest error in predicting the cross-sectional area is generated in the largest size classes. However, the estimation error in scatterer cross-sectional area is greater for the smaller size classes because of the great number of smaller particles.

The total scatterer cross-sectional area estimated from the size class midpoint value for diameter is about 1.7 times as large as the total cross-sectional area estimated from the average measured volume (Table 9). Hence, cross-sectional area calculations should be made from measured volume values. The total cross-sectional area of scatterers per volume of sediment is given at the bottom of Table 9. X-radiograph core 20 has twice the potential scattering area of the other samples due to the greater number of scatterers. The calculated scatterer cross-sectional area is the maximum available area that the particles can potentially provide. The significant cross-sectional area of scatterers is a function of orientation and concentration of the particles within the sediment volume. An orientation factor to adjust the maximum potential area to a realized area would take into account such sedimentological phenomena as graded bedding and such biological activity as bioturbation. Graded bedding would tend to deposit flat scatterers with the greatest area exposed toward the incident acoustic energy. Reworking of the sediment by burrowing infauna tend to diminish the potential area even more by producing a random orientation of scatterers (Richardson et al., 1983). Concentration is an important factor to a certain level, beyond which an increase in the number of scatterers does not increase the total cross-sectional area because of shadowing. However, very large scatterers would not have to be

Table 9. Values of scatterer cross-sectional area (mm³) for box core 17 and x-radiograph cores 18 and 20 calculated from the size class midpoint value for particle diameter ($\bar{d}$-area) and the average measured volume of the particles ($\bar{V}$-area). The respective total cross-sectional areas in each size class are based on the number of particles from Table 7.

Class Midpoint	$\bar{d}$-area	total	$\bar{v}$-area	total	$\bar{d}$-area	total	$\bar{v}$-area	total	$\bar{d}$-area	total	$\bar{v}$-area	total
20.75	338	1691	104	519								
17.45	239	1913	77.2	618								
14.67	169	1859	57.0	627	169	338	96.2	192	169	338	164	327
12.34	120	5023	72.6	3051	120	120	119	119	120	598	89.2	446
10.37	84.5	8784	57.5	5981	84.5	507	61.7	370	84.5	1182	45.4	636
8.72	59.7	12,362	43.1	8917	59.7	836	44.1	618	59.7	2090	42.0	1471
7.34	42.3	22,046	29.5	15,366	42.3	1777	30.5	1280	42.3	3766	29.8	2655
6.17	29.9	18,747	20.9	13,147	29.9	1375	23.8	1093	29.9	2930	21.1	2068
5.19	21.2	28,179	14.2	18,887	21.2	2898	16.7	2283	21.2	4570	15.3	3302
4.36	14.9	52,077	10.0	34,972	14.9	3852	10.9	2819	14.9	6375	10.8	4631
3.67	10.6	66,793	7.48	47,225	10.6	6432	7.22	4387	10.6	9732	7.18	6608
3.08	7.45	118,735	4.60	73,361	7.45	11,637	4.66	7280	7.45	13,947	4.89	9152
2.59	5.27	235,625	2.94	103,289	5.27	19,072	2.84	10,275	5.27	24,446	2.75	12,758
2.18	3.73	165,900	2.17	96,566	3.73	17,388	2.01	9346	3.73	24,812	1.96	13,001
TOTAL		739,734		422,526		66,232		40,062		94,786		57,055
AREA/VOLUME		0.02		0.01		0.02		0.01		0.04		0.02

present in great numbers to reach the maximum available cross-sectional area for scattering.

The RMS height roughness value is ideal as a model input for the Arafura Sea experiment because the average value for the power spectral slope from pathlengths approaching 100 cm (71.4 cm) is the same as the basic assumption of the model. However, for use of the model in general the power spectral slope does not always attain a propitious value of -2.25. In those cases where the power spectral slope is greater (absolute value), such as a bottom with ripples, or smaller, such as a bottom with a high spatial frequency roughness, a model input for power spectral slope is appropriate. Another advantageous feature of the sea floor at the Arafura Sea experiment site is the lack of roughness anisotropy. In a ripple field where there is roughness anisotropy, the two-dimensional roughness power spectrum is not an appropriate model input. As the model is currently written, an estimate of the two-dimensional power spectrum is made from the ideal value of -2.25 for the one-dimensional power spectrum. This shortcoming of the model probably has a negligible effect on the ability of the model to predict backscattering strength from the experiment site in the Arafura Sea. Scattering of acoustic energy from this bottom is predominantly from the sediment volume rather than the sediment surface.

Conclusions

The experiment site in the Arafura Sea is ideally suited for investigation of sediment volume scattering. The sea floor is relatively homogeneous with respect to physical properties and small- and large-scale roughness. Although some variability exists in the concentration of potential scatterers in and on the sea floor, these variations are evidently insignificant in their effect on acoustic bottom backscattering. Due to the low values of density and velocity ratios characteristic of soft, or muddy, sediments, the roughness of the sea floor at the experiment site is not a significant factor in scattering sound. However, the large amounts of mollusk shells and shell fragments embedded in the sediment are considered to be the source of the high, constant level of measured backscattering intensity. When an arbitrary value of 0.005 is used for sediment volume scattering parameter instead of the default value, the simplified composite roughness model fits the measured data well. The inability of the model to accurately predict the scattering intensity at small grazing angles (Jackson, 1987a) may be related to biogenic effects. The presence of mats of fauna and/or flora and mounds of reworked sediment on the surface of the sea floor could create a greater bottom loss, or absorption of sound than a comparable, less biologically active sea floor. Measurements of the sediment volume scatterers give consistent values for scatterer weight, volume, density,

and shape. Determination of scatterer orientation is complicated by the fact that x-radiograph cores show only one aspect of the scatterer orientation definitively. In future investigations, horizontally oriented x-radiograph cores should be collected to observe the orientation aspect significant to the incident sound. The results of this experiment also suggest that beyond a certain concentration of scatterers, additional scatterers may not add significantly to the level of scattering intensity.

This investigation provides valuable information on the characteristics of sediment-entrained volume scatterers in the soft sediment of the Arafura Sea. The descriptions of the scatterer "population" in this report will be used to formulate new approaches to sediment volume scattering in the composite roughness model. Now that the scatterers are characterized to the best of our available technical ability, a Rayleigh scattering model or geometric optics approximation (appropriate to predict sediment volume scattering from these data) may be applied to the data. To properly use this database for the improvement or augmentation of existing scattering models, we need to design scattering experiments in areas with scatterers of different concentration and character. In addition, we advocate laboratory experiments be conducted with variable concentrations of volume scatterers embedded in test sediments. Further work is required to discern where sediment roughness scattering starts to dominate sediment volume scattering in the spectrum of sediment types existing in shallow-water environments.

References

Balke, B. and D. Burt (1976). Arafura Sea area. In *Economic Geology of Australia and Papua New Guinea*, R.B. Leslie, H.J. Evans and C.L. Knight (eds.), v. 3, Petroleum, Australas. Inst. Min. Metall., Monogr. Ser., no. 7, pp. 209-212.

Bloomfield, P. (1976). *Fourier Analysis of Time Series: An Introduction*. John Wiley & Sons, New York, NY.

Briggs, K. B. and M. D. Richardson (1984). *Physical and Acoustical Properties of Surface Sediment from Venezuela Basin: A Data Report*. Naval Ocean Research and Development Activity, Stennis Space Center, MS, NORDA Tech. Note 238, 282 pp.

Briggs, K. B., P. Fleischer, R. I. Ray, W. B. Sawyer, D. K. Young, M. D. Richardson, and S. Stanic (1986). *Environmental Support for a High-frequency Acoustic Bottom Backscatter Experiment off Charleston, South Carolina, 17-28 June 1983*. Naval Ocean Research and Development Activity, Stennis Space Center, MS, NORDA Report 130, 90 pp.

Curray, J. R., G. G. Shor, Jr., R. W. Raitt, and M. Henry (1977). Seismic refraction and reflection studies of crustal structure of the eastern Sunda and western Banda Arcs. *J. Geophys. Res.* 82, 2479-2489.

Folk, R. L. (1965). *Petrology of Sedimentary Rocks.* Hemphill's, Austin, TX.

Hamilton, E. L. (1970). Reflection coefficients and bottom losses at normal incidence computed from Pacific sediment properties. *Geophysics* 35, 995-1004.

Hamilton, E. L. (1971). Sound velocity and related properties of marine sediments, North Pacific. *J. Geophys. Res.* 75, 4423-4446.

Hamilton, E. L. (1972). Compressional wave attenuation in marine sediments. *Geophysics* 37, 620-646.

Hovland, M. (1981). Characteristics of pockmarks in the Norwegian Trench. *Mar. Geol.* 39, 103-117.

Jackson, D. R. (1986). *High-frequency Bottom Backscattering in the Arafura Sea.* APL-University of Washington, Seattle, WA, APL-UW Report 5-86, 37 pp.

Jackson, D. R. (1987a). *Vertical-incidence Bottom Backscattering in the Arafura Sea.* APL-University of Washington, Seattle, WA, APL-UW Report 2-87, 21 pp.

Jackson, D. R. (1987b). *Third Report on TTCP Bottom Scattering Measurements: Model Development.* APL-University of Washington, Seattle, WA, APL-UW Report 8708, 110 pp.

Jackson, D. R. and M. D. Richardson (1985). High-frequency bottom backscattering in the Arafura Sea. *J. Acoust. Soc. Am.* Suppl. 78, S59.

Jackson, D.R. and K.B. Briggs. (1987). Model and data comparisons for bottom backscattering. *J. Acoust. Soc. Am.* Suppl. 82, S122.

Jackson, D. R., D. P. Winebrenner, and A. Ishimaru (1986). Application of the composite roughness model to high-frequency bottom backscattering. *J. Acoust. Soc. Am.* 79, 1410-1422.

Jongsma, D. (1974). Marine geology of the Arafura Sea. Department of Minerals and Energy, Bureau of Mineral Resources, Australian Govt. Publ. Serv., Canberra, *Geology and Geophysics Bull.* 157, 76 pp.

King, L. H. and B. MacLean (1970). Pockmarks on the Scotian Shelf. *Geol. Soc. America Bull.* 81, 3141-3148.

Lambert, D. N. and R. H. Bennett (1972). *Tables for Determining Porosity of Deep-sea Sediments from Water Content and Average Grain Density Measurements.* NOAA Technical Memo., ERL AOML-17, 57 pp.

Neurauter, T. W. (1979). *Bed Forms on the Florida Shelf as Detected with Side Scan Sonar.* M.S. Thesis, Univ. of South Florida, St. Petersburg, 125 p.

Phipps, C. V. G. (1967). The character and evolution of the Australian continental shelf. *Aust. Pet. Explor. Assoc. J.*, 7 (II), 44-49.

Richardson, M. D. (1986). Spatial variability of surficial shallow water sediment geoacoustic properties. In *Ocean Seismo-Acoustics,* T. Akal and J.M. Berkson (eds.), Plenum Press, New York, NY.

Richardson, M. D., D. K. Young, and K. B. Briggs (1983). Effects of hydrodynamic and biological processes on sediment geoacoustic properties in Long Island Sound, USA. *Mar. Geol.* 52, 201-226.

Richardson, M. D., K. B. Briggs, R. I. Ray, and W. H. Jahn (1986). *Environmental Support for High-frequency Acoustic Experiments Conducted at the Quinault Range, April-May 1983.* Naval Ocean Research and Development Activity, NORDA Report 132, Stennis Space Center, MS, 76 pp.

Stanic, S., P. Fleischer, K. B. Briggs, M. D. Richardson, and B. Eckstein (1987). *High-frequency Acoustic Bottom Scattering Experiments, Part I: Instrumentation and Methods.* Naval Ocean Research and Development Activity, NORDA Report 178, Stennis Space Center, MS, 47 pp.

Tjia, H. D. (1966). Arafura Sea. In *The Encylopedia of Oceanography,* R. W. Fairbridge (ed.), Dowden, Hutchinson & Ross, Stroudsburg, pp. 44-47.

Whiticar, M. J. and F. Werner (1981). Pockmarks: Submarine vents of natural gas or freshwater seeps? *Geo-Marine Lett.* 1, 193-199.

Appendix A1

Geoacoustic Data at 125 kHz

Geoacoustic and physical property data from sediments collected from the Arafura Sea. Compressional wave velocity (*Vp*), velocity ratio (*Vp* ratio), and compressional wave attenuation (alpha and k) determined at 125 kHz. Mean grain size (φ) determined for one subcore per box core; sediment porosity (Pors.) determined for two subcores per box core.

31

Cruise: HMAS COOK   Station: 17-1   Date: 5/18/84
Position: 10-01S;137-50E   Depth: 47m

Calculated for: 23.6   Deg-C   35.00 o/oo   0 m   125 kHz

Depth (cm)	Vp (m/sec)	Vp Ratio	Alpha (dB/m)	Attenuation k	MGS (0)	MGS (mm)	% Pors	Dens (g/cc)	AGD (g/cc)
WATER	1528.5	0.999	0.0	0.000					
0.0	1520.1	0.994	10.6	0.084					
1.0	1515.6	0.991	34.3	0.275					
2.0	1519.3	0.993	34.3	0.275					
3.0	1517.1	0.992	47.9	0.383					
4.0	1507.3	0.986	62.9	0.503					
5.0	1511.1	0.988	62.9	0.503					
6.0	1496.2	0.978	62.9	0.503					
7.0	1490.4	0.974	111.5	0.892					
8.0	1499.5	0.980	164.8	1.318					
9.0	1505.8	0.985	116.0	0.928					
10.0	1505.8	0.985	116.0	0.928					
11.0	1512.6	0.989	62.9	0.503					
12.0	1511.1	0.988	79.7	0.637					
13.0	1510.7	0.988	62.9	0.503					
14.0	1520.1	0.994	55.2	0.442					
15.0	1512.2	0.989	193.4	1.547					
16.0	1508.8	0.987	111.5	0.892					
17.0	1511.4	0.988	94.7	0.757					
18.0	1510.3	0.988	62.9	0.503					
19.0	1510.3	0.988	47.9	0.383					
20.0	1508.8	0.987	47.9	0.383					
21.0	1505.8	0.985	71.1	0.568					

PRINTOUT DATE: 29 Mar 1988

Cruise: HMAS COOK   Station: 17-2   Date: 5/18/84
Position: 10-01S;137-50E   Depth: 47m

Calculated for: 23.6 Deg-C   35.00 o/oo   0 m   125 kHz

Depth (cm)	Vp (m/sec)	Vp Ratio	Alpha (dB/m)	Attenuation k	MGS (0)	MGS (mm)	% Pors	Dens (g/cc)	AGD (g/cc)
WATER	1528.1	0.999	0.0	0.000					
0.0	1522.8	0.996	5.2	0.041					
1.0	1511.4	0.988	21.9	0.176	5.11	0.03	77.1		
2.0	1513.3	0.989	34.3	0.275					
3.0	1511.4	0.988	34.3	0.275	5.36	0.02	74.4		
4.0	1511.4	0.988	34.3	0.275					
5.0	1511.8	0.989	34.3	0.275	5.42	0.02	73.3		
6.0	1509.2	0.987	47.9	0.383					
7.0	1506.2	0.985	55.2	0.442	5.07	0.03	68.6		
8.0	1509.6	0.987	47.9	0.383					
9.0	1507.3	0.986	41.0	0.328	4.93	0.03	69.6		
10.0	1509.9	0.987	55.2	0.442					
11.0	1509.9	0.987	47.9	0.383	5.77	0.02	70.8		
12.0	1508.1	0.986	34.3	0.275					
13.0	1508.1	0.986	41.0	0.328	6.09	0.01	68.3		
14.0	1505.8	0.985	41.0	0.328					
15.0	1509.9	0.987	47.9	0.383	5.27	0.03	68.5		
16.0	1505.8	0.985	47.9	0.383					
17.0	1504.4	0.984	34.3	0.275	6.85	0.01	72.4		
18.0	1502.1	0.982	28.0	0.224					
19.0	1504.0	0.983	47.9	0.383	6.15	0.01	68.5		
20.0	1509.6	0.987	34.3	0.275					
21.0	1509.6	0.987	47.9	0.383	6.03	0.02	68.8		
22.0	1507.3	0.986	62.9	0.503					
23.0	1511.1	0.988	62.9	0.503	5.10	0.03	68.0		
24.0	1507.3	0.986	71.1	0.568					
25.0					6.06	0.01	63.9		
26.0									
27.0					5.92	0.02	68.1		
28.0									
29.0					5.65	0.02	69.0		

33

PRINTOUT DATE: 29 Mar 1988

Cruise: HMAS COOK   Station: 17-3   Date: 5/18/84
Position: 10-01S;137-50E   Depth: 47m

Calculated for: 23.6   Deg-C   35.00 o/oo   0 m   125 kHz

Depth (cm)	Vp (m/sec)	Vp Ratio	Alpha (dB/m)	Attenuation k	MGS (Ø)	MGS (mm)	% Pors	Dens (g/cc)	AGD (g/cc)
WATER	1529.2	1.000	0.0	0.000					
0.0	1524.7	0.997	0.0	0.000					
1.0	1516.7	0.992	10.6	0.084			78.4		
2.0	1513.7	0.990	34.3	0.275					
3.0	1513.7	0.990	47.9	0.383			73.5		
4.0	1508.1	0.986	34.3	0.275					
5.0	1503.6	0.983	34.3	0.275			73.5		
6.0	1505.8	0.985	34.3	0.275					
7.0	1507.3	0.986	62.9	0.503			71.8		
8.0	1503.6	0.983	79.7	0.637					
9.0	1513.7	0.990	62.9	0.503			67.7		
10.0	1505.1	0.984	62.9	0.503					
11.0	1507.0	0.985	79.7	0.637			67.3		
12.0	1514.8	0.990	47.9	0.383					
13.0	1512.6	0.989	41.0	0.328			68.2		
14.0	1507.3	0.986	34.3	0.275					
15.0	1507.3	0.986	34.3	0.275			69.2		
16.0	1507.0	0.985	47.9	0.383					
17.0	1510.7	0.988	41.0	0.328			71.2		
18.0	1505.5	0.984	41.0	0.328					
19.0	1512.9	0.989	47.9	0.383			68.3		
20.0	1510.7	0.988	55.2	0.442					
21.0	1513.7	0.990	47.9	0.383			66.7		
22.0	1508.1	0.986	34.3	0.275					
23.0	1506.6	0.985	34.3	0.275			68.3		
24.0	1510.3	0.988	34.3	0.275					
25.0	1510.3	0.988	62.9	0.503			69.9		
26.0	1511.1	0.988	47.9	0.383					
27.0	1509.9	0.987	79.7	0.637			69.1		
28.0	1517.4	0.992	55.2	0.442					
29.0	1525.8	0.998	111.5	0.892			68.4		
30.0	1492.2	0.976	201.5	1.612					
31.0							70.4		

PRINTOUT DATE: 29 Mar 1988

Cruise: HMAS COOK   Station: 18-1   Date: 5/18/84
Position: 10-01S;137-50E   Depth: 47m

Calculated for: 23.0   Deg-C   35.00 o/oo   0 m   125 kHz

Depth (cm)	Vp (m/sec)	Vp Ratio	Alpha (dB/m)	Attenuation k	MGS (θ)	MGS (mm)	% Pors	Dens (g/cc)	AGD (g/cc)
WATER	1529.3	1.000	0.0	0.000					
0.0	1520.2	0.994	10.6	0.084					
1.0	1506.3	0.985	16.1	0.129					
2.0	1503.3	0.983	10.6	0.084					
3.0	1506.3	0.985	34.3	0.275					
4.0	1506.7	0.985	34.3	0.275					
5.0	1505.9	0.985	41.0	0.328					
6.0	1504.1	0.983	28.0	0.224					
7.0	1500.0	0.981	21.9	0.176					
8.0	1508.9	0.987	41.0	0.328					
9.0	1512.6	0.989	94.7	0.757					
10.0	1520.2	0.994	79.7	0.637					
11.0	1514.1	0.990	47.9	0.383					
12.0	1511.1	0.988	62.9	0.503					
13.0	1513.0	0.989	55.2	0.442					
14.0	1509.3	0.987	47.9	0.383					
15.0	1510.4	0.988	41.0	0.328					
16.0	1511.5	0.988	47.9	0.383					
17.0	1518.7	0.993	47.9	0.383					
18.0	1519.8	0.994	62.9	0.503					
19.0	1519.4	0.993	79.7	0.637					
20.0	1509.6	0.987	79.7	0.637					
21.0	1518.3	0.993	62.9	0.503					
22.0	1515.3	0.991	47.9	0.383					
23.0	1516.8	0.992	71.1	0.568					
24.0	1518.7	0.993	62.9	0.503					
25.0	1512.6	0.989	62.9	0.503					
26.0	1511.1	0.988	34.3	0.275					
27.0	1510.4	0.988	34.3	0.275					
28.0	1504.8	0.984	34.3	0.275					
29.0	1501.5	0.982	34.3	0.275					
30.0	1502.2	0.982	28.0	0.224					
31.0	1504.4	0.984	47.9	0.383					
32.0	1517.5	0.992	71.1	0.568					

Cruise: HMAS COOK   Station: 18-2   Date: 5/18/84
Position: 10-01S;137-50E   Depth: 47m

Calculated for: 23.0   Deg-C   35.00 o/oo   0 m   125 kHz

Depth (cm)	Vp (m/sec)	Vp Ratio	Alpha (dB/m)	Attenu ation k	MGS (0)	MGS (mm)	% Pors	Dens (g/cc)	AGD (g/cc)
1.0	1505.5	0.984	5.2	0.041			83.7		
2.0	1503.3	0.983	16.1	0.129					
3.0	1504.1	0.983	28.0	0.224			75.0		
4.0	1511.1	0.988	47.9	0.383					
5.0	1508.9	0.987	79.7	0.637			75.2		
6.0	1510.0	0.987	34.3	0.275					
7.0	1509.3	0.987	41.0	0.328			69.6		
8.0	1506.7	0.985	34.3	0.275					
9.0	1505.5	0.984	34.3	0.275			68.1		
10.0	1505.9	0.985	28.0	0.224					
11.0	1506.7	0.985	34.3	0.275			71.7		
12.0	1507.8	0.986	34.3	0.275					
13.0	1505.2	0.984	41.0	0.328			73.4		
14.0	1504.8	0.984	34.3	0.275					
15.0	1507.8	0.986	34.3	0.275			70.7		
16.0	1507.0	0.985	34.3	0.275					
17.0	1509.3	0.987	34.3	0.275			68.4		
18.0	1513.4	0.990	62.9	0.503					
19.0	1516.0	0.991	55.2	0.442			69.0		
20.0	1517.1	0.992	79.7	0.637					
21.0	1513.4	0.990	79.7	0.637			66.2		
22.0	1536.2	1.004	79.7	0.637					
23.0	1541.7	1.008	120.6	0.965			64.9		
24.0	1546.4	1.011	87.0	0.696					
25.0	1541.7	1.008	76.2	0.609			66.1		
26.0	1524.3	0.997	94.7	0.757					
27.0	1513.4	0.990	87.0	0.696			68.7		
28.0	1506.7	0.985	71.1	0.568					
29.0	1502.6	0.982	47.9	0.383			70.1		
30.0	1500.0	0.981	55.2	0.442					
31.0	1509.3	0.987	55.2	0.442			67.8		
32.0	1510.4	0.988	62.9	0.503					
33.0	1513.4	0.990	62.9	0.503			66.6		
34.0	1513.0	0.989	71.1	0.568					
35.0	1511.5	0.988	62.9	0.503			71.9		
36.0	1507.4	0.986	62.9	0.503					

Cruise: HMAS COOK   Station: 18-3   Date: 5/18/84
Position: 10-01S;137-50E   Depth: 47m

Calculated for: 23.6   Deg-C   35.00 o/oo   0 m   125 kHz

Depth (cm)	Vp (m/sec)	Vp Ratio	Alpha (dB/m)	Attenuation k	MGS (θ)	MGS (mm)	% Pors	Dens (g/cc)	AGD (g/cc)
1.0	1513.6	0.990	21.9	0.176	6.46	0.01	80.0		
2.0	1511.7	0.988	34.3	0.275					
3.0	1515.5	0.991	34.3	0.275	5.57	0.02	72.0		
4.0	1512.5	0.989	55.2	0.442					
5.0	1512.5	0.989	55.2	0.442	5.85	0.02	69.9		
6.0	1506.1	0.985	34.3	0.275					
7.0	1506.1	0.985	34.3	0.275	6.95	0.01	70.7		
8.0	1512.1	0.989	47.9	0.383					
9.0	1509.5	0.987	47.9	0.383	5.00	0.03	69.4		
10.0	1510.2	0.987	90.8	0.726					
11.0	1493.6	0.977	102.8	0.823	4.86	0.03	70.8		
12.0	1515.1	0.991	79.7	0.637					
13.0	1518.1	0.993	90.8	0.726	4.38	0.05	70.1		
14.0	1495.8	0.978	193.4	1.547					
15.0	1488.1	0.973	210.2	1.681	5.11	0.03	62.9		
16.0	1511.3	0.988	111.5	0.892					
17.0	1518.9	0.993	62.9	0.503	5.48	0.02	69.8		
18.0	1515.8	0.991	71.1	0.568					
19.0	1500.5	0.981	79.7	0.637	5.63	0.02	66.1		
20.0	1514.7	0.990	62.9	0.503					
21.0	1520.0	0.994	62.9	0.503	5.01	0.03	68.1		
22.0	1520.8	0.994	79.7	0.637					
23.0	1523.8	0.996	90.8	0.726	5.40	0.02	67.7		
24.0	1522.3	0.995	62.9	0.503					
25.0	1520.4	0.994	62.9	0.503	5.15	0.03	68.6		
26.0	1516.6	0.992	79.7	0.637					
27.0	1521.9	0.995	98.7	0.790	4.78	0.04	70.3		
28.0	1520.4	0.994	62.9	0.503					
29.0	1512.5	0.989	62.9	0.503	5.49	0.02	70.8		
30.0	1503.5	0.983	71.1	0.568					
31.0	1503.9	0.983	79.7	0.637	6.59	0.01	70.0		
32.0	1511.0	0.988	41.0	0.328					
33.0	1512.1	0.989	47.9	0.383	5.43	0.02	67.9		
34.0	1511.3	0.988	47.9	0.383					
35.0	1512.8	0.989	71.1	0.568	5.86	0.02	68.2		
36.0	1515.1	0.991	55.2	0.442					

Cruise: HMAS COOK   Station: 19-1   Date: 5/18/84
Position: 10-01S;137-50E   Depth: 47m

Calculated for: 23.8   Deg-C   35.00 o/oo   0 m   125 kHz

Depth (cm)	Vp (m/sec)	Vp Ratio	Alpha (dB/m)	Attenuation k	MGS (0)	MGS (mm)	% Pors	Dens (g/cc)	AGD (g/cc)
WATER	1528.8	1.000	0.0	0.000					
0.0	1522.7	0.996	0.0	0.000					
1.0	1510.2	0.987	10.6	0.084					
2.0	1505.7	0.985	16.1	0.129					
3.0	1503.5	0.983	21.9	0.176					
4.0	1508.0	0.986	28.0	0.224					
5.0	1506.1	0.985	34.3	0.275					
6.0	1508.7	0.986	41.0	0.328					
7.0	1512.5	0.989	47.9	0.383					
8.0	1510.2	0.987	41.0	0.328					
9.0	1512.5	0.989	47.9	0.383					
10.0	1519.6	0.994	62.9	0.503					
11.0	1520.0	0.994	71.1	0.568					
12.0	1521.1	0.995	62.9	0.503					
13.0	1513.2	0.989	47.9	0.383					
14.0	1510.2	0.987	34.3	0.275					
15.0	1509.8	0.987	71.1	0.568					
16.0	1508.0	0.986	130.5	1.044					
17.0	1509.8	0.987	130.5	1.044					
18.0	1515.5	0.991	71.1	0.568					
19.0	1508.0	0.986	41.0	0.328					
20.0	1512.5	0.989	55.2	0.442					
21.0	1508.0	0.986	79.7	0.637					
22.0	1511.3	0.988	55.2	0.442					
23.0	1508.7	0.986	41.0	0.328					
24.0	1496.5	0.978	88.9	0.711					
25.0	1505.4	0.984	90.8	0.726					
26.0	1508.0	0.986	47.9	0.383					
27.0	1505.4	0.984	41.0	0.328					
28.0	1509.8	0.987	79.7	0.637					
29.0	1518.1	0.993	79.7	0.637					
30.0	1515.1	0.991	71.1	0.568					
31.0	1514.7	0.990	141.0	1.128					

Cruise: HMAS COOK   Station: 19-2   Date: 5/18/84
Position: 10-01S;137-50E   Depth: 47m

Calculated for: 23.6   Deg-C   35.00 o/oo   0 m   125 kHz

Depth (cm)	Vp (m/sec)	Vp Ratio	Alpha (dB/m)	Attenuation k	MGS (0)	MGS (mm)	% Pors	Dens (g/cc)	AGD (g/cc)
WATER	1526.3	0.998	0.0	0.000					
0.0	1519.1	0.993	5.2	0.041					
1.0	1507.1	0.985	16.1	0.129	6.91	0.01	81.0		
2.0	1501.8	0.982	34.3	0.275					
3.0	1501.5	0.982	34.3	0.275	6.10	0.01	78.1		
4.0	1505.9	0.985	34.3	0.275					
5.0	1504.8	0.984	34.3	0.275	5.03	0.03	76.4		
6.0	1505.6	0.984	47.9	0.383					
7.0	1509.7	0.987	34.3	0.275	5.22	0.03	72.9		
8.0	1508.5	0.986	41.0	0.328					
9.0	1505.2	0.984	62.9	0.503	5.20	0.03	73.5		
10.0	1514.2	0.990	71.1	0.568					
11.0	1516.8	0.992	55.2	0.442	4.57	0.04	65.3		
12.0	1518.3	0.993	62.9	0.503					
13.0	1520.2	0.994	79.7	0.637	5.17	0.03	64.6		
14.0	1519.5	0.994	71.1	0.568					
15.0	1514.5	0.990	47.9	0.383	5.89	0.02	66.3		
16.0	1521.4	0.995	62.9	0.503					
17.0	1514.5	0.990	79.7	0.637	4.86	0.03	64.2		
18.0	1509.7	0.987	62.9	0.503					
19.0	1508.9	0.987	62.9	0.503	5.14	0.03	69.0		
20.0	1513.4	0.990	79.7	0.637					
21.0	1513.4	0.990	62.9	0.503	5.33	0.02	67.8		
22.0	1508.9	0.987	47.9	0.383					
23.0	1505.2	0.984	55.2	0.442	5.72	0.02	69.3		
24.0	1506.7	0.985	47.9	0.383					
25.0	1506.3	0.985	55.2	0.442	5.42	0.02	71.3		
26.0	1509.3	0.987	55.2	0.442					
27.0	1504.8	0.984	62.9	0.503	5.64	0.02	69.0		
28.0	1509.7	0.987	55.2	0.442					
29.0	1511.5	0.988	62.9	0.503	5.21	0.03	66.8		
30.0	1507.4	0.986	79.7	0.637					
31.0					4.65	0.04	67.1		

Cruise: HMAS COOK   Station: 19-3   Date: 5/18/84
Position: 10-01S;137-50E   Depth: 47m

Calculated for: 23.0   Deg-C   35.00 o/oo   0 m   125 kHz

Depth (cm)	Vp (m/sec)	Vp Ratio	Alpha (dB/m)	Attenuation k	MGS (0)	MGS (mm)	% Pors	Dens (g/cc)	AGD (g/cc)
WATER	1526.3	0.998	0.0	0.000					
0.0	1514.2	0.990	10.6	0.084					
1.0	1503.0	0.983	16.1	0.129			82.7		
2.0	1498.9	0.980	21.9	0.175					
3.0	1500.0	0.981	28.0	0.224			78.5		
4.0	1497.0	0.979	41.0	0.328					
5.0	1498.2	0.980	34.3	0.275			77.4		
6.0	1499.3	0.980	34.3	0.275					
7.0	1496.7	0.979	28.0	0.224			76.8		
8.0	1499.3	0.980	34.3	0.275					
9.0	1502.2	0.982	47.9	0.383			73.0		
10.0	1505.6	0.984	47.9	0.383					
11.0	1509.3	0.987	47.9	0.383			69.8		
12.0	1515.7	0.991	62.9	0.503					
13.0	1512.3	0.989	71.1	0.568			68.1		
14.0	1507.4	0.986	71.1	0.568					
15.0	1507.1	0.985	55.2	0.442			68.1		
16.0	1505.2	0.984	47.9	0.383					
17.0	1509.7	0.987	71.1	0.568			66.9		
18.0	1512.7	0.989	71.1	0.568					
19.0	1508.2	0.986	55.2	0.442			64.4		
20.0	1513.4	0.990	79.7	0.637					
21.0	1515.3	0.991	71.1	0.568			64.6		
22.0	1519.8	0.994	71.1	0.568					
23.0	1523.6	0.996	98.7	0.790			64.1		
24.0	1516.4	0.992	98.7	0.790					
25.0	1510.0	0.987	62.9	0.503			66.2		
26.0	1504.1	0.983	79.7	0.637					
27.0	1504.8	0.984	71.1	0.568			68.4		
28.0	1509.7	0.987	111.5	0.892					
29.0	1499.6	0.981	79.7	0.637			69.2		
30.0	1503.7	0.983	87.0	0.696					
31.0	1500.0	0.981	41.0	0.328			69.0		
32.0	1497.4	0.979	41.0	0.328					

PRINTOUT DATE: 29 Mar 1988

Cruise: HMAS COOK   Station: 20-1   Date: 5/18/84
Position: 10-01S;137-50E   Depth: 47m

Calculated for: 23.6 Deg-C   35.00 o/oo   0 m   125 kHz

Depth (cm)	Vp (m/sec)	Vp Ratio	Alpha (dB/m)	Attenuation k	MGS (θ)	MGS (mm)	% Pors	Dens (g/cc)	AGD (g/cc)
WATER	1526.3	0.998	0.0	0.000					
0.0	1522.9	0.996	10.6	0.084					
1.0	1520.2	0.994	41.0	0.328	4.11	0.06	71.6		
2.0	1525.5	0.997	79.7	0.637					
3.0	1527.1	0.998	62.9	0.503	3.79	0.07	64.3		
4.0	1531.7	1.002	94.7	0.757					
5.0	1542.2	1.008	135.7	1.085	3.28	0.10	62.4		
6.0	1554.0	1.016	87.0	0.696					
7.0	1554.0	1.016	94.7	0.757	3.13	0.11	63.4		
8.0	1541.0	1.008	102.8	0.823					
9.0	1538.3	1.006	98.7	0.790	3.48	0.09	64.9		
10.0	1530.5	1.001	76.2	0.609					
11.0	1527.1	0.998	71.1	0.568	4.67	0.04	68.0		
12.0	1525.2	0.997	62.9	0.503					
13.0	1525.9	0.998	79.7	0.637	4.81	0.04	66.4		
14.0	1523.6	0.996	62.9	0.503					
15.0	1516.4	0.992	55.2	0.442	4.74	0.04	63.6		
16.0	1514.5	0.990	79.7	0.637					
17.0	1513.0	0.989	79.7	0.637	5.42	0.02	70.3		
18.0	1507.8	0.986	47.9	0.383					
19.0	1505.6	0.984	62.9	0.503	5.18	0.03	65.2		
20.0	1514.2	0.990	79.7	0.637					
21.0	1514.2	0.990	79.7	0.637	5.35	0.02	69.8		
22.0	1511.5	0.988	55.2	0.442					
23.0	1510.0	0.987	34.3	0.275	4.85	0.03	69.9		
24.0	1508.9	0.987	55.2	0.442					
25.0	1507.1	0.985	62.9	0.503	4.03	0.06	67.9		
26.0	1504.1	0.983	79.7	0.637					
27.0	1511.2	0.988	130.5	1.044	5.73	0.02	69.6		
28.0	1523.3	0.996	125.5	1.044					
29.0	1508.9	0.987	83.3	0.666	5.04	0.03	70.1		
30.0	1504.1	0.983	62.9	0.503					
31.0	1504.1	0.983	79.7	0.637	4.81	0.04	68.6		
32.0	1504.4	0.984	111.5	0.892					
33.0	1500.4	0.981	135.7	1.085	5.28	0.03	68.3		

41

Cruise: HMAS COOK   Station: 20-2   Date: 5/18/84
Position: 10-01S;137-50E   Depth: 47m

Calculated for: 23.0   Deg-C   35.00 o/oo   0 m   125 kHz

Depth (cm)	Vp (m/sec)	Vp Ratio	Alpha (dB/m)	Attenuation k	MGS (0)	MGS (mm)	% Pors	Dens (g/cc)	AGD (g/cc)
WATER	1525.9	0.998	0.0	0.000					
0.0	1516.1	0.991	10.6	0.084					
1.0	1511.9	0.989	10.6	0.084					
2.0	1511.9	0.989	34.3	0.275					
3.0	1521.4	0.995	98.7	0.790					
4.0	1525.5	0.997	125.5	1.004					
5.0	1544.1	1.010	116.0	0.928					
6.0	1546.1	1.011	79.7	0.637					
7.0	1540.6	1.007	107.1	0.857					
8.0	1529.0	1.000	87.0	0.696					
9.0	1521.4	0.995	55.2	0.442					
10.0	1517.9	0.993	62.9	0.503					
11.0	1517.9	0.993	55.2	0.442					
12.0	1512.7	0.989	79.7	0.637					
13.0	1498.9	0.980	130.5	1.044					
14.0	1498.9	0.980	146.6	1.173					
15.0	1506.3	0.985	102.8	0.823					
16.0	1503.3	0.983	55.2	0.442					
17.0	1502.6	0.982	41.0	0.328					
18.0	1506.7	0.985	79.7	0.637					
19.0	1513.0	0.989	72.7	0.582					
20.0	1515.3	0.991	62.9	0.503					
21.0	1512.7	0.989	71.1	0.568					
22.0	1508.2	0.986	47.9	0.383					
23.0	1508.9	0.987	62.9	0.503					
24.0	1510.8	0.988	71.1	0.568					
25.0	1514.5	0.990	62.9	0.503					
26.0	1515.7	0.991	62.9	0.503					
27.0	1512.3	0.989	90.8	0.726					
28.0	1518.7	0.993	90.8	0.726					
29.0	1513.0	0.989	71.1	0.568					
30.0	1512.3	0.989	79.7	0.637					
31.0	1508.9	0.987	130.5	1.044					

Cruise: HMAS COOK   Station: 20-3   Date: 5/18/84
Position: 10-01S;137-50E   Depth: 47m

Calculated for: 23.6   Deg-C   35.00 o/oo   0 m   125 kHz

Depth (cm)	Vp (m/sec)	Vp Ratio	Alpha (dB/m)	Attenuation k	MGS (Ø)	MGS (mm)	% Pors	Dens (g/cc)	AGD (g/cc)
WATER	1526.7	0.998	0.0	0.000					
0.0	1525.2	0.997	10.6	0.084					
1.0	1525.2	0.997	47.9	0.383			67.6		
2.0	1536.7	1.005	79.7	0.637					
3.0	1534.0	1.003	79.7	0.637			62.1		
4.0	1537.1	1.005	79.7	0.637					
5.0	1532.1	1.002	71.1	0.568			66.9		
6.0	1530.9	1.001	79.7	0.637					
7.0	1535.5	1.004	79.7	0.637			63.7		
8.0	1528.6	0.999	62.9	0.503					
9.0	1525.2	0.997	55.2	0.442			67.1		
10.0	1521.0	0.995	62.9	0.503					
11.0	1516.8	0.992	47.9	0.383			71.3		
12.0	1513.8	0.990	28.0	0.224					
13.0	1509.7	0.987	71.1	0.568			67.0		
14.0	1512.3	0.989	55.2	0.442					
15.0	1508.9	0.987	28.0	0.224			68.1		
16.0	1501.8	0.982	34.3	0.275					
17.0	1507.1	0.985	47.9	0.383			74.5		
18.0	1506.3	0.985	62.9	0.503					
19.0	1507.8	0.986	47.9	0.383			74.8		
20.0	1506.7	0.985	62.9	0.503					
21.0	1509.3	0.987	55.2	0.442			68.8		
22.0	1512.7	0.989	55.2	0.442					
23.0	1514.5	0.990	94.7	0.757			65.2		
24.0	1508.9	0.987	90.8	0.726					
25.0	1507.1	0.985	62.9	0.503			69.5		
26.0	1505.6	0.984	55.2	0.442					
27.0	1502.2	0.982	62.9	0.503			69.2		
28.0	1505.9	0.985	47.9	0.383					
29.0	1504.1	0.983	34.3	0.275			70.6		
30.0	1504.8	0.984	41.0	0.328					
31.0	1510.8	0.988	62.9	0.503			71.5		
32.0	1510.8	0.988	79.7	0.637					
33.0	1513.8	0.990	79.7	0.637			68.5		
34.0	1512.3	0.989	111.5	0.892					

Appendix A2

Geoacoustic Data at 400 kHz

Geoacoustic data from sediments collected from the Arafura Sea. Compressional wave velocity (*Vp*), velocity ratio (*Vp* ratio), and compressional wave attenuation (alpha and k) determined at 400 kHz.

CRUISE: HMAS COOK   STATION: 17-1   DATE: 18 MAY 1984
   LAT: 10-01S   LONG: 137-50E   DEPTH: 47
   CALCULATED FOR: 23.0 DEG-C   35.0 o/oo   0 m   400 kHz

DEPTH(CM)	Vp(M/SEC)	Vp RATIO	ALPHA (dB/M)	k
-1.0	1525.3	.997	0.0	0.000
0.0	1517.7	.992	74.9	.187
1.0	1510.6	.988	189.8	.475
2.0	1511.7	.988	194.6	.487
3.0	1515.8	.991	304.1	.760
4.0	1511.7	.988	283.7	.709
5.0	1507.6	.986	216.8	.542
6.0	1503.5	.983	250.0	.625
7.0	1507.6	.986	512.9	1.282
8.0	1505.4	.984	426.6	1.066
9.0	1505.7	.985	341.4	.854
10.0	1513.2	.989	512.9	1.282
11.0	1512.5	.989	402.8	1.007
12.0	1514.0	.990	341.4	.854
13.0	1512.5	.989	373.2	.933
14.0	1509.5	.987	373.2	.933
15.0	1506.9	.985	440.1	1.100
16.0	1509.8	.987	364.6	.911
17.0	1504.6	.984	392.2	.981
18.0	1507.6	.986	382.4	.956
19.0	1511.3	.988	315.5	.789
20.0	1512.8	.989	309.7	.774
21.0	1512.8	.989	373.2	.933
22.0	1506.1	.985	364.6	.911

```
CRUISE: HMAS COOK          STATION:   17-2          DATE: 18 MAY 1984
    LAT:        10-01S         LONG: 137-50E        DEPTH: 47
    CALCULATED FOR:        23.0 DEG-C        35.0 o/oo        0 m        400 kHz


        DEPTH(CM)       Vp(M/SEC)      Vp RATIO      ALPHA (dB/M)          k
          -1.0           1525.9          .998           0.0            0.000
           0.0           1520.2          .994          74.9            .187
           1.0           1510.8          .988         211.0            .527
           2.0           1512.6          .989         222.8            .557
           3.0           1512.6          .989         242.7            .607
           4.0           1510.0          .987         211.0            .527
           5.0           1510.0          .987         229.2            .573
           6.0           1508.5          .986         283.7            .709
           7.0           1502.2          .982         440.1           1.100
           8.0           1504.4          .984         440.1           1.100
           9.0           1506.7          .985         392.2            .981
          10.0           1513.4          .990         414.2           1.035
          11.0           1508.9          .987         229.2            .573
          12.0           1507.8          .986         229.2            .573
          13.0           1507.8          .986         235.8            .589
          14.0           1506.3          .985         283.7            .709
          15.0           1509.6          .987         283.7            .709
          16.0           1511.5          .988         382.4            .956
          17.0           1505.5          .984         382.4            .956
          18.0           1503.7          .983         309.7            .774
          19.0           1508.2          .986         321.5            .804
          20.0           1509.6          .987         348.7            .872
          21.0           1510.4          .988         298.7            .747
          22.0           1508.5          .986         382.4            .956
          23.0           1509.3          .987         327.9            .820
          24.0           1505.5          .984         334.5            .836
          25.0           1503.3          .983         348.7            .872
          26.0           1504.4          .984         293.5            .734
```

DEPTH(CM)	Vp(M/SEC)	Vp RATIO	ALPHA (dB/M)	k
-1.0	1525.3	.997	0.0	0.000
0.0	1523.8	.996	28.6	.071
1.0	1513.6	.990	64.4	.161
2.0	1513.2	.989	222.8	.557
3.0	1513.6	.990	242.7	.607
4.0	1511.0	.988	194.8	.487
5.0	1508.7	.986	175.8	.440
6.0	1506.8	.985	180.3	.451
7.0	1511.0	.988	205.4	.513
8.0	1513.2	.989	341.4	.854
9.0	1512.5	.989	265.9	.665
10.0	1510.2	.987	283.7	.709
11.0	1516.6	.992	341.4	.854
12.0	1513.2	.989	426.6	1.066
13.0	1505.7	.985	327.9	.820
14.0	1508.3	.986	293.5	.734
15.0	1506.5	.985	304.1	.760
16.0	1510.2	.987	283.7	.709
17.0	1506.1	.985	261.8	.654
18.0	1504.6	.984	341.4	.854
19.0	1505.7	.985	348.7	.872
20.0	1511.7	.988	373.2	.933
21.0	1515.1	.991	288.5	.721
22.0	1509.8	.987	327.9	.820
23.0	1508.0	.986	257.7	.644
24.0	1510.6	.988	279.0	.698
25.0	1509.1	.987	321.5	.804
26.0	1506.5	.985	304.1	.760
27.0	1511.3	.988	373.2	.933
28.0	1515.5	.991	364.6	.911
29.0	1516.6	.992	402.8	1.007
30.0	1520.4	.994	501.5	1.254
31.0	1504.6	.984	512.9	1.282
32.0	1506.8	.985	414.2	1.035

```
CRUISE: HMAS COOK          STATION:    18-1         DATE: 18 MAY 1984
    LAT:      10-01S          LONG: 137-50E       DEPTH: 47
    CALCULATED FOR:      23.0 DEG-C          35.0 o/oo          0 m        400 kHz


    DEPTH(CM)     Vp(M/SEC)     Vp RATIO     ALPHA (dB/M)         k
      -1.0        1526.1         .998            0.0           0.000
       0.0        1520.8         .994           38.7            .097
       1.0        1506.8         .985          105.6            .264
       2.0        1507.2         .986          137.4            .344
       3.0        1509.5         .987          216.2            .541
       4.0        1510.2         .987          198.8            .497
       5.0        1509.5         .987          188.2            .471
       6.0        1506.5         .985          188.2            .471
       7.0        1506.8         .985          137.4            .344
       8.0        1507.6         .986          210.2            .525
       9.0        1512.5         .989          297.5            .744
      10.0        1512.5         .989          272.4            .681
      11.0        1514.0         .990          303.0            .758
      12.0        1506.8         .985          321.2            .803
      13.0        1512.5         .989          327.9            .820
      14.0        1514.0         .990          308.9            .772
      15.0        1516.6         .992          303.0            .758
      16.0        1514.7         .990          321.2            .803
      17.0        1514.7         .990          396.2            .990
      18.0        1518.5         .993          407.6           1.019
      19.0        1516.2         .991          366.6            .916
      20.0        1509.5         .987          494.9           1.237
      21.0        1515.5         .991          448.5           1.121
      22.0        1514.0         .990          396.2            .990
      23.0        1518.1         .993          433.5           1.084
      24.0        1515.1         .991          419.9           1.050
      25.0        1515.8         .991          334.8            .837
      26.0        1513.2         .989          292.1            .730
      27.0        1511.0         .988          267.9            .670
      28.0        1511.0         .988          277.1            .693
      29.0        1505.7         .985          229.2            .573
      30.0        1504.6         .984          210.2            .525
      31.0        1503.9         .983          204.3            .511
      32.0        1511.3         .988          222.5            .556
      33.0        1518.5         .993          236.1            .590
      34.0        1520.4         .994          308.9            .772
```

49

DEPTH(CM)	Vp(M/SEC)	Vp RATIO	ALPHA (dB/M)	k
-1.0	1524.6	.997	14.3	.036
0.0	1517.0	.992	73.9	.185
1.0	1506.1	.985	178.4	.446
2.0	1506.8	.985	193.4	.483
3.0	1510.2	.987	229.2	.573
4.0	1516.6	.992	297.5	.744
5.0	1516.2	.991	251.1	.628
6.0	1514.0	.990	229.2	.573
7.0	1510.6	.988	178.4	.446
8.0	1508.7	.986	210.2	.525
9.0	1505.4	.984	216.2	.541
10.0	1507.6	.986	222.5	.556
11.0	1509.8	.987	216.2	.541
12.0	1508.3	.986	210.2	.525
13.0	1508.3	.986	229.2	.573
13.0	1508.3	.986	229.2	.573
14.0	1505.7	.985	259.3	.648
15.0	1508.3	.986	251.1	.628
16.0	1506.8	.985	286.9	.717
17.0	1511.0	.988	267.9	.670
18.0	1521.1	.995	314.9	.787
19.0	1518.9	.993	407.6	1.019
20.0	1514.7	.990	385.6	.964
21.0	1514.7	.990	448.5	1.121
22.0	1521.1	.995	292.1	.730
23.0	1526.8	.998	433.5	1.084
24.0	1533.8	1.003	703.6	1.759
25.0	1523.4	.996	321.2	.803
26.0	1512.1	.989	342.1	.855
27.0	1507.6	.986	277.1	.693
28.0	1507.6	.986	236.1	.590
29.0	1508.7	.986	277.1	.693
30.0	1512.1	.989	297.5	.744
31.0	1513.2	.989	349.8	.875
32.0	1511.3	.988	474.5	1.186
33.0	1512.5	.989	506.3	1.266
34.0	1510.2	.987	448.5	1.121
35.0	1511.3	.988	267.9	.670
36.0	1509.8	.987	251.1	.628
37.0	1509.8	.987	385.6	.964
38.0	1511.7	.988	286.9	.717
39.0	1509.8	.987	281.9	.705

dry.ξ

50

CRUISE: HMAS COOK   STATION: 18-3   DATE: 18 MAY 1984
    LAT: 10-01S   LONG: 137-50E   DEPTH: 47
    CALCULATED FOR: 23.0 DEG-C   35.0 o/oo   0 m   400 kHz

DEPTH(CM)	Vp(M/SEC)	Vp RATIO	ALPHA (dB/M)	k
-1.0	1527.2	.999	0.0	0.000
0.0	1521.5	.995	47.9	.120
1.0	1511.3	.988	73.9	.185
2.0	1511.3	.988	210.2	.525
3.0	1513.6	.990	243.4	.609
4.0	1514.0	.990	259.3	.648
5.0	1516.2	.991	314.9	.787
6.0	1511.7	.988	267.9	.670
7.0	1507.2	.986	193.4	.483
8.0	1509.5	.987	210.2	.525
9.0	1511.0	.988	321.2	.803
10.0	1507.6	.986	308.9	.772
11.0	1499.1	.980	456.7	1.142
12.0	1508.7	.986	308.9	.772
13.0	1512.8	.989	321.2	.803
14.0	1507.2	.986	465.3	1.163
15.0	1500.2	.981	532.2	1.331
16.0	1504.6	.984	433.5	1.084
17.0	1514.3	.990	390.8	.977
18.0	1520.0	.994	342.1	.855
19.0	1513.6	.990	342.1	.855
20.0	1514.0	.990	292.1	.730
21.0	1516.2	.991	321.2	.803
22.0	1517.7	.992	375.8	.939
23.0	1517.7	.992	456.7	1.142
24.0	1516.2	.991	362.2	.906
25.0	1514.0	.990	292.1	.730
26.0	1515.8	.991	358.0	.895
27.0	1515.8	.991	518.6	1.297
28.0	1511.3	.988	506.3	1.266
29.0	1502.8	.983	308.9	.772
30.0	1503.9	.983	236.1	.590
31.0	1505.7	.985	267.9	.670
32.0	1507.2	.986	222.5	.556
33.0	1506.1	.985	210.2	.525
34.0	1508.7	.986	349.8	.875
35.0	1512.1	.989	321.2	.803
36.0	1504.6	.984	263.5	.659
37.0	1507.2	.986	321.2	.803

```
CRUISE: HMAS COOK        STATION:   19-1          DATE: 18 MAY 1984
   LAT:     10-01S          LONG: 137-50E        DEPTH: 47
   CALCULATED FOR:        23.0 DEG-C          35.0 o/oo          0 m        400 kHz


   DEPTH(CM)       Vp(M/SEC)       Vp RATIO       ALPHA (dB/M)          k
     -1.0           1525.0          .997             0.0            0.000
      0.0           1519.6          .994            38.7             .097
      1.0           1509.5          .987            85.7             .214
      2.0           1506.1          .985           105.6             .264
      3.0           1506.9          .985           105.6             .264
      4.0           1508.7          .986           137.4             .344
      5.0           1509.8          .987           251.1             .628
      6.0           1507.6          .986           327.9             .820
      7.0           1506.5          .985           334.8             .837
      8.0           1503.9          .983           366.6             .916
      9.0           1507.2          .986           407.6            1.019
     10.0           1511.7          .988           419.9            1.050
     11.0           1515.5          .991           366.6             .916
     12.0           1513.2          .989           349.8             .875
     13.0           1508.0          .986           396.2             .990
     14.0           1509.5          .987           303.0             .758
     15.0           1508.0          .986           385.6             .964
     16.0           1510.2          .987           506.3            1.266
     17.0           1505.0          .984           401.7            1.004
     18.0           1505.4          .984           255.1             .638
     19.0           1505.0          .984           236.1             .590
     20.0           1505.0          .984           286.9             .717
     21.0           1507.2          .986           327.9             .820
     22.0           1503.1          .983           292.1             .730
     23.0           1501.7          .982           236.1             .590
     24.0           1505.4          .984           263.5             .659
     25.0           1503.9          .983           308.9             .772
     26.0           1500.5          .981           297.5             .744
     27.0           1499.4          .980           277.1             .693
     28.0           1504.6          .984           334.8             .837
     29.0           1508.4          .986           327.9             .820
     30.0           1505.4          .984           263.5             .659
     31.0           1508.4          .986           236.1             .590
     32.0           1512.1          .989           303.0             .758
```

52

```
CRUISE: HMAS COOK        STATION:    19-2        DATE: 18 MAY 1984
   LAT:      10-01S          LONG: 137-50E        DEPTH: 47
   CALCULATED FOR:        23.0 DEG-C          35.0 o/oo          0 m        400 kHz


   DEPTH(CM)        Vp(M/SEC)        Vp RATIO        ALPHA (dB/M)            k
      -1.0            1524.2           .997             327.9             .820
       0.0            1517.7           .992              47.9             .120
       1.0            1507.2           .986             105.6             .264
       2.0            1506.1           .985             137.4             .344
       3.0            1506.9           .985             120.6             .302
       4.0            1506.9           .985             169.2             .423
       5.0            1505.7           .985             222.5             .556
       6.0            1502.0           .982             334.8             .837
       7.0            1505.0           .984             327.9             .820
       8.0            1503.1           .983             247.2             .618
       9.0            1504.6           .984             222.5             .556
      10.0            1507.2           .986             297.5             .744
      11.0            1507.2           .986             494.9            1.237
      12.0            1513.6           .990             761.4            1.903
      13.0            1529.9          1.000             583.0            1.458
      14.0            1525.0           .997             494.9            1.237
      15.0            1511.0           .988             474.5            1.186
      16.0            1515.1           .991             375.8             .939
      17.0            1517.7           .992             532.2            1.331
      18.0            1508.0           .986             366.6             .916
      19.0            1504.6           .984             342.1             .855
      20.0            1509.5           .987             433.5            1.084
      21.0            1507.2           .986             358.0             .895
      22.0            1509.1           .987             334.8             .837
      23.0            1507.6           .986             334.8             .837
      24.0            1506.1           .985             259.3             .648
      25.0            1503.9           .983             321.2             .803
      26.0            1510.2           .987             303.0             .758
      27.0            1519.3           .993             349.8             .875
      28.0            1519.3           .993             349.8             .875
      29.0            1515.1           .991             375.8             .939
      30.0            1508.0           .986             349.8             .875
```

DEPTH(CM)	Vp(M/SEC)	Vp RATIO	ALPHA (dB/M)	k
-1.0	1524.6	.997	0.0	0.000
0.0	1511.7	.988	72.7	.182
1.0	1505.7	.985	91.8	.229
2.0	1503.5	.983	134.1	.335
3.0	1502.8	.983	153.6	.384
4.0	1499.8	.981	222.2	.556
5.0	1499.8	.981	222.2	.556
6.0	1502.4	.982	153.6	.384
7.0	1500.5	.981	171.4	.429
8.0	1503.1	.983	215.6	.539
9.0	1504.6	.984	327.9	.820
10.0	1508.4	.986	290.5	.726
11.0	1509.8	.987	342.9	.857
12.0	1515.1	.991	406.7	1.017
13.0	1507.2	.986	419.6	1.049
14.0	1505.4	.984	413.0	1.032
15.0	1505.4	.984	280.0	.700
16.0	1507.6	.986	327.9	.820
17.0	1511.3	.988	400.6	1.002
18.0	1511.3	.988	342.9	.857
19.0	1511.0	.988	368.8	.922
20.0	1514.4	.990	351.0	.878
21.0	1512.1	.989	598.0	1.495
22.0	1520.4	.994	487.9	1.220
23.0	1529.6	1.000	499.3	1.248
24.0	1518.5	.993	499.3	1.248
25.0	1505.7	.985	346.9	.867
26.0	1505.7	.985	314.3	.786
27.0	1504.6	.984	426.6	1.066
28.0	1504.6	.984	441.6	1.104
29.0	1500.9	.981	467.5	1.169
30.0	1507.6	.986	327.9	.820
31.0	1504.3	.984	256.6	.641
32.0	1501.7	.982	203.2	.508

```
CRUISE: HMAS COOK        STATION:    20-1          DATE: 18 MAY 1984
   LAT:      10-01S           LONG: 137-50E        DEPTH: 47
   CALCULATED FOR:      23.0 DEG-C         35.0 o/oo          0 m        400 kHz


     DEPTH(CM)        Vp(M/SEC)       Vp RATIO       ALPHA (dB/M)          k
        -1.0           1525.4           .997            0.0             0.000
         0.0           1522.4           .995           113.7             .284
         1.0           1521.6           .995           351.0             .878
         2.0           1519.7           .994           525.3            1.313
         3.0           1521.2           .995           394.8             .987
         4.0           1521.6           .995           540.3            1.351
         5.0           1527.0           .998           557.0            1.393
         6.0           1525.0           .997           624.0            1.560
         7.0           1525.8           .998           576.1            1.440
         8.0           1519.0           .993           624.0            1.560
         9.0           1512.9           .989           624.0            1.560
        10.0           1517.8           .992           499.3            1.248
        11.0           1522.4           .995           413.0            1.032
        12.0           1517.8           .992           426.6            1.066
        13.0           1522.0           .995           449.7            1.124
        14.0           1519.7           .994           378.7             .947
        15.0           1513.7           .990           394.8             .987
        16.0           1509.5           .987           441.6            1.104
        17.0           1509.5           .987           400.6            1.002
        18.0           1507.7           .986           244.2             .610
        19.0           1505.8           .985           314.3             .786
        20.0           1512.5           .989           389.2             .973
        21.0           1509.2           .987           389.2             .973
        22.0           1505.1           .984           229.2             .573
        23.0           1504.3           .984           296.1             .740
        24.0           1513.7           .990           290.5             .726
        25.0           1517.8           .992           335.2             .838
        26.0           1513.7           .990           525.3            1.313
        27.0           1508.4           .986           458.3            1.146
        28.0           1504.7           .984           346.9             .867
        29.0           1505.9           .985           296.1             .740
        30.0           1507.3           .986           320.9             .801
        31.0           1504.3           .984           359.6             .899
        32.0           1509.2           .987           525.3            1.313
```

```
CRUISE: HMAS COOK        STATION:    20-2         DATE: 18 MAY 1984
   LAT:      10-01S           LONG: 137-50E       DEPTH: 47
   CALCULATED FOR:       23.0 DEG-C        35.0 o/oo          0 m       400 kHz


      DEPTH(CM)      Vp(M/SEC)      Vp RATIO      ALPHA (dB/M)         k
        -1.0          1524.6          .997           0.0            0.000
         0.0          1517.7          .992          78.8             .197
         1.0          1508.0          .986         139.7             .349
         2.0          1509.8          .987         222.2             .556
         3.0          1511.7          .988         389.2             .973
         4.0          1512.8          .989         458.3            1.146
         5.0          1512.8          .989         458.3            1.146
         6.0          1510.6          .988         853.1            2.133
         7.0          1517.7          .992         624.0            1.560
         8.0          1512.1          .989         458.3            1.146
         9.0          1508.0          .986         346.9             .867
        10.0          1511.0          .988         339.0             .847
        11.0          1513.6          .990         335.2             .838
        12.0          1512.5          .989         378.7             .947
        13.0          1502.0          .982         598.0            1.495
        14.0          1497.2          .979         624.0            1.560
        15.0          1502.4          .982         413.0            1.032
        16.0          1502.8          .983         229.2             .573
        17.0          1503.9          .983         215.6             .539
        18.0          1513.2          .989         327.9             .820
        19.0          1512.8          .989         487.9            1.220
        20.0          1511.7          .988         413.0            1.032
        21.0          1515.5          .991         383.8             .960
        22.0          1510.2          .987         327.9             .820
        23.0          1509.8          .987         351.0             .878
        24.0          1514.0          .990         426.6            1.066
        25.0          1516.2          .991         400.6            1.002
        26.0          1516.2          .991         389.2             .973
        27.0          1514.0          .990         480.6            1.202
        28.0          1517.4          .992         346.9             .867
        29.0          1514.4          .990         335.2             .838
        30.0          1511.0          .988         327.9             .820
        31.0          1508.9          .985         499.3            1.248
```

CRUISE: HMAS COOK   STATION: 20-3   DATE: 18 MAY 1984
   LAT: 10-01S   LONG: 137-50E   DEPTH: 47
   CALCULATED FOR: 23.0 DEG-C   35.0 o/oo   0 m   400 kHz
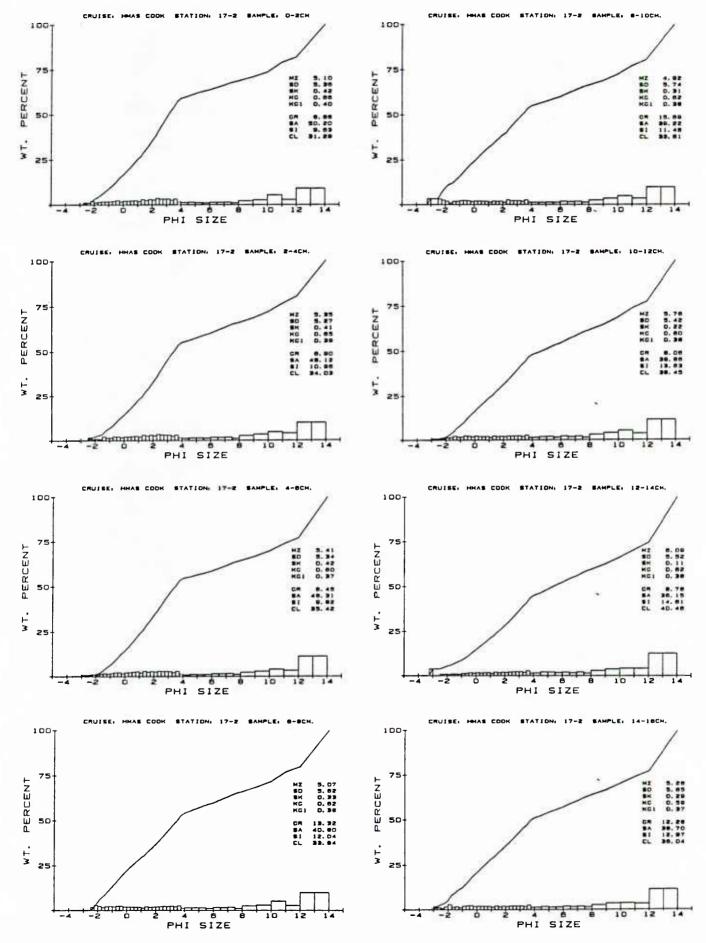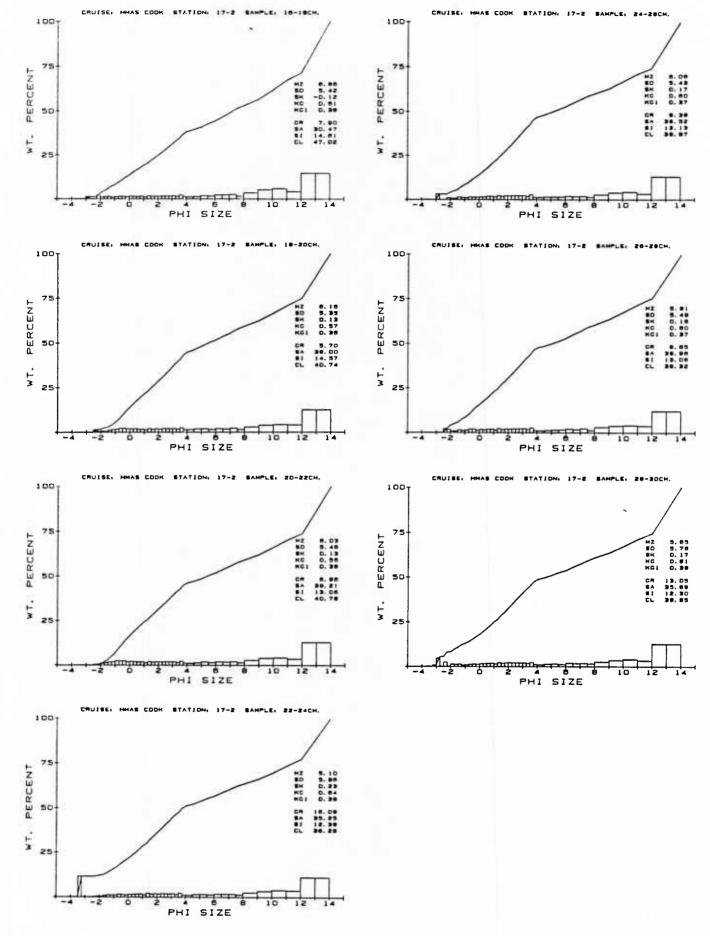
DEPTH(CM)	Vp(M/SEC)	Vp RATIO	ALPHA (dB/M)	k
-1.0	1526.1	.998	0.0	0.000
0.0	1523.1	.996	139.7	.349
1.0	1514.0	.990	433.9	1.085
2.0	1518.5	.993	525.3	1.313
3.0	1518.5	.993	557.0	1.393
4.0	1525.4	.997	426.6	1.066
5.0	1520.0	.994	406.7	1.017
6.0	1520.0	.994	477.4	1.193
7.0	1524.6	.997	598.0	1.495
8.0	1512.5	.989	477.4	1.193
9.0	1515.1	.991	400.6	1.002
10.0	1514.0	.990	413.0	1.032
11.0	1511.7	.988	314.3	.786
12.0	1511.7	.988	256.6	.641
13.0	1510.6	.988	327.9	.820
14.0	1506.9	.985	215.6	.539
15.0	1504.6	.984	171.4	.429
16.0	1505.7	.985	244.2	.610
17.0	1505.7	.985	270.1	.675
18.0	1509.8	.987	378.7	.947
19.0	1505.0	.984	285.1	.713
20.0	1505.0	.984	290.5	.726
21.0	1505.0	.984	308.0	.770
22.0	1509.8	.987	327.9	.820
23.0	1506.5	.985	359.6	.899
24.0	1502.4	.982	433.9	1.085
25.0	1510.6	.988	301.9	.755
26.0	1505.0	.984	314.3	.786
27.0	1505.0	.984	314.3	.786
28.0	1506.1	.985	320.9	.802
29.0	1506.1	.985	301.9	.755
30.0	1504.3	.984	320.9	.802
31.0	1509.8	.987	301.9	.755
32.0	1509.8	.987	270.1	.675
33.0	1510.2	.987	229.2	.573
34.0	1514.0	.990	280.0	.700
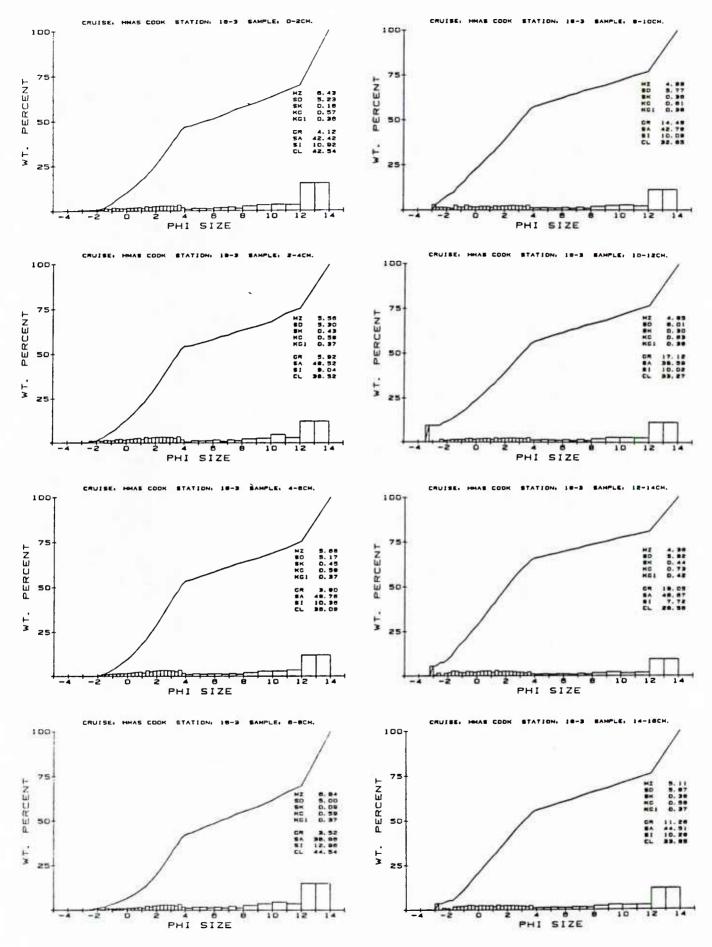
Appendix B
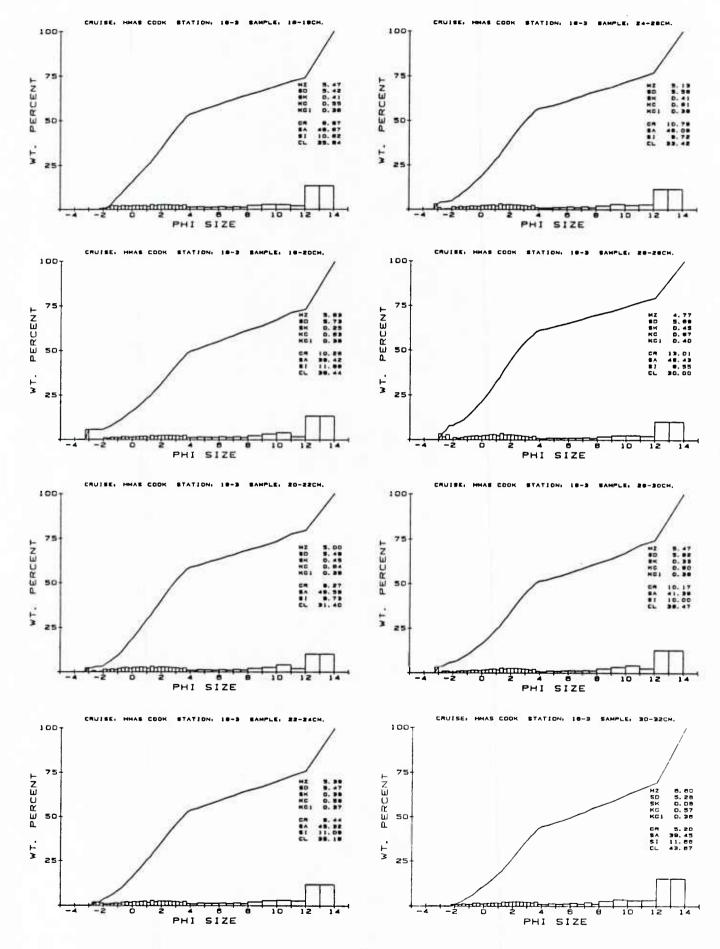
Sediment Grain-Size Frequency Histograms
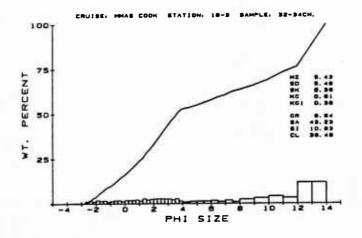
Sediment grain-size distribution data from 2-cm intervals expressed as frequency histograms, mean grain diameter (*MZ*), sorting coefficient (*SD*), skewness (*SK*), kurtosis (*KG*), normalized kurtosis (*KG1*), and percent gravel, sand, silt, and clay.

CRUISE: HMAS COOK STATION: 17-2 SAMPLE: 16-18CM.

MZ 8.88
SD 5.42
SK -0.12
KG 0.61
KG1 0.38

GR 7.90
SA 30.47
SI 14.61
CL 47.02

CRUISE: HMAS COOK STATION: 17-2 SAMPLE: 24-26CM.

MZ 8.08
SD 5.43
SK 0.17
KG 0.60
KG1 0.37

GR 8.38
SA 38.52
SI 13.13
CL 38.97

CRUISE: HMAS COOK STATION: 17-2 SAMPLE: 18-20CM.

MZ 8.16
SD 5.35
SK 0.13
KG 0.57
KG1 0.38

GR 5.70
SA 39.00
SI 14.57
CL 40.74

CRUISE: HMAS COOK STATION: 17-2 SAMPLE: 26-28CM.

MZ 5.91
SD 5.49
SK 0.18
KG 0.60
KG1 0.37

GR 8.65
SA 38.98
SI 13.06
CL 38.32

CRUISE: HMAS COOK STATION: 17-2 SAMPLE: 20-22CM.

MZ 8.03
SD 5.48
SK 0.13
KG 0.55
KG1 0.38

GR 8.95
SA 38.21
SI 12.06
CL 40.78

CRUISE: HMAS COOK STATION: 17-2 SAMPLE: 28-30CM.

MZ 5.65
SD 5.78
SK 0.17
KG 0.61
KG1 0.38

GR 13.05
SA 35.69
SI 12.30
CL 38.85

CRUISE: HMAS COOK STATION: 17-2 SAMPLE: 22-24CM.

MZ 5.10
SD 5.95
SK 0.23
KG 0.64
KG1 0.39

GR 16.09
SA 35.25
SI 12.39
CL 36.29

61

CRUISE: HMAS COOK STATION: 10-3 SAMPLE: 16-18CM.

CRUISE: HMAS COOK STATION: 10-3 SAMPLE: 24-26CM.

CRUISE: HMAS COOK STATION: 10-3 SAMPLE: 18-20CM.

CRUISE: HMAS COOK STATION: 10-3 SAMPLE: 26-28CM.

CRUISE: HMAS COOK STATION: 10-3 SAMPLE: 20-22CM.

CRUISE: HMAS COOK STATION: 10-3 SAMPLE: 28-30CM.

CRUISE: HMAS COOK STATION: 10-3 SAMPLE: 22-24CM.

CRUISE: HMAS COOK STATION: 10-3 SAMPLE: 30-32CM.

63

CRUISE: HMAS COOK STATION: 16-3 SAMPLE: 32-34CM.

CRUISE: HMAS COOK STATION: 16-3 SAMPLE: 34-36CM.

CRUISE: HMAS COOK STATION: 16-3 SAMPLE: 36-38CM.

64

65

CRUISE: HMAS COOK   STATION: 19-2   SAMPLE: 16-18CM.
CRUISE: HMAS COOK   STATION: 19-2   SAMPLE: 24-26CM.
CRUISE: HMAS COOK   STATION: 19-2   SAMPLE: 18-20CM.
CRUISE: HMAS COOK   STATION: 19-2   SAMPLE: 26-28CM.
CRUISE: HMAS COOK   STATION: 19-2   SAMPLE: 20-22CM.
CRUISE: HMAS COOK   STATION: 19-2   SAMPLE: 28-30CM.
CRUISE: HMAS COOK   STATION: 19-2   SAMPLE: 22-24CM.
CRUISE: HMAS COOK   STATION: 19-2   SAMPLE: 30-32CM.

66

68

CRUISE: HMAS COOK   STATION: 20-1   SAMPLE: 32-34CM.

MZ	5.29
SD	5.90
SK	0.24
KG	0.59
KG1	0.37
GR	14.90
SA	35.59
SI	10.26
CL	39.25

Appendix C1

Bottom Roughness Height Data
for 35.56-cm Pathlengths

Relative sediment height versus pathlength for orientations A-C (N-S) and D-F (E-W) in the 12 stereo photographs from 35.56-cm pathlengths.

ARA 2-67 F
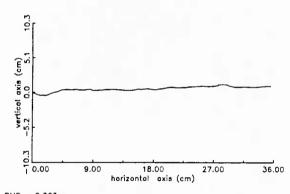
RMS = 0.230 cm
Max elev. diff. in prof. : 0.985

ARA 2-67 E
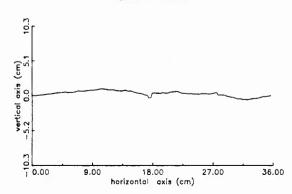
RMS = 0.165 cm
Max elev. diff. in prof. : 0.745

ARA 2-67 D
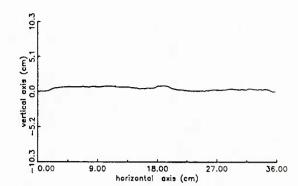
RMS = 0.363 cm
Max elev. diff. in prof. : 1.676

ARA 2-67 C
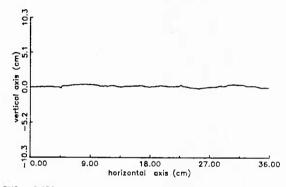
RMS = 0.397 cm
Max elev. diff. in prof. : 1.576

ARA 2-67 B
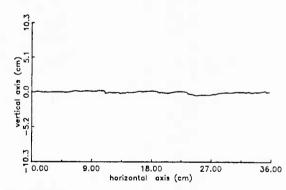
RMS = 0.240 cm
Max elev. diff. in prof. : 0.848

ARA 2-67 A
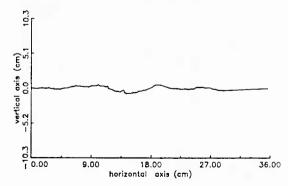
RMS = 0.139 cm
Max elev. diff. in prof. : 0.660

ARA 2-63 F
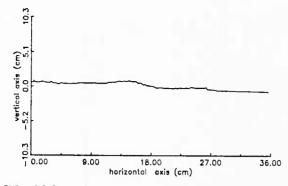
RMS = 0.162 cm
Max elev. diff. in prof. : 0.729

ARA 2-63 E
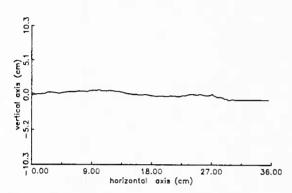
RMS = 0.277 cm
Max elev. diff. in prof. : 1.382

72

ARA 2-63 D
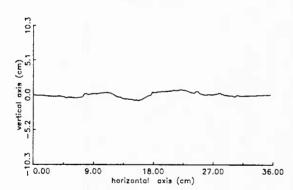
RMS = 0.515 cm
Max elev. diff. in prof. : 1.612

ARA 2-47 F

RMS = 0.279 cm
Max elev. diff. in prof. : 1.041

ARA 2-63 C

RMS = 0.443 cm
Max elev. diff. in prof. : 1.546


ARA 2-47 E
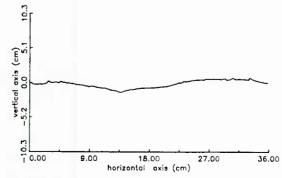
RMS = 0.730 cm
Max elev. diff. in prof. : 2.499

ARA 2-63 B

RMS = 0.367 cm
Max elev. diff. in prof. : 1.639

ARA 2-47 D
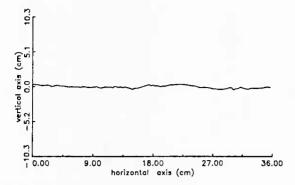
RMS = 0.461 cm
Max elev. diff. in prof. : 1.754

ARA 2-63 A

RMS = 0.177 cm
Max elev. diff. in prof. : 0.828

ARA 2-47 C
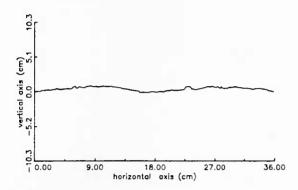
RMS = 0.575 cm
Max elev. diff. in prof. : 2.155

73

ARA 2-47 B
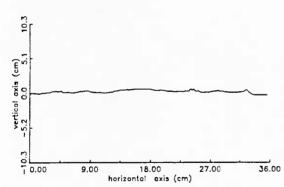
RMS = 0.204 cm
Max elev. diff. in prof. : 0.811

ARA 2-47 A
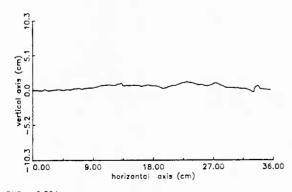
RMS = 0.270 cm
Max elev. diff. in prof. : 1.030

ARA 2-43 F
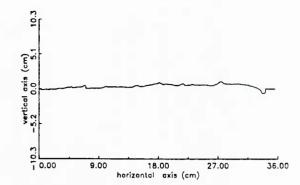
RMS = 0.219 cm
Max elev. diff. in prof. : 0.895

ARA 2-43 E
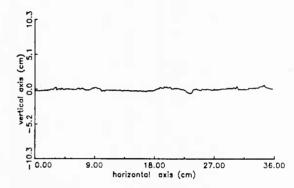
RMS = 0.354 cm
Max elev. diff. in prof. : 1.569

ARA 2-43 D
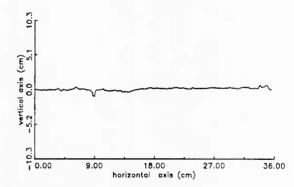
RMS = 0.320 cm
Max elev. diff. in prof. : 1.750

ARA 2-43 C
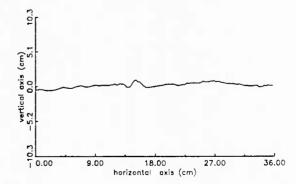
RMS = 0.196 cm
Max elev. diff. in prof. : 1.265

ARA 2-43 B
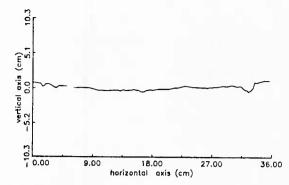
RMS = 0.215 cm
Max elev. diff. in prof. : 1.661

ARA 2-43 A
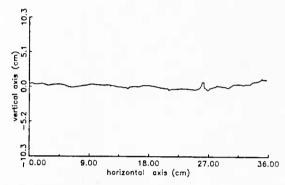
RMS = 0.349 cm
Max elev. diff. in prof. : 1.548

74

ARA 2-42 F
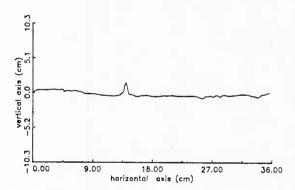
RMS = 0.382 cm
Max elev. diff. in prof. : 1.699

ARA 2-42 B

RMS = 0.283 cm
Max elev. diff. in prof. : 1.905

ARA 2-42 E

RMS = 0.321 cm
Max elev. diff. in prof. : 1.679

ARA 2-42 A
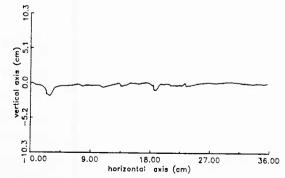
RMS = 0.253 cm
Max elev. diff. in prof. : 1.357

ARA 2-42 D

RMS = 0.378 cm
Max elev. diff. in prof. : 2.305

ARA 2-32 F
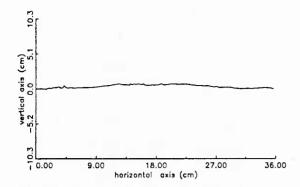
RMS = 0.551 cm
Max elev. diff. in prof. : 2.553

ARA 2-42 C

RMS = 0.453 cm
Max elev. diff. in prof. : 1.701

ARA 2-32 E
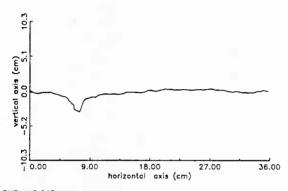
RMS = 0.342 cm
Max elev. diff. in prof. : 2.134

75

ARA 2-32 D
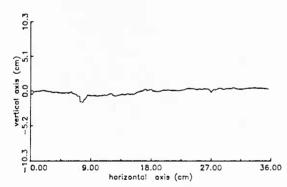
RMS = 0.250 cm
Max elev. diff. in prof. : 0.848

ARA 2-32 C
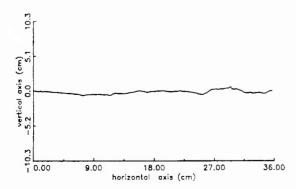
RMS = 0.645 cm
Max elev. diff. in prof. : 3.412

ARA 2-32 B
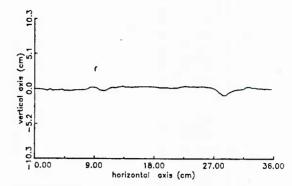
RMS = 0.424 cm
Max elev. diff. in prof. : 2.131

ARA 2-32 A
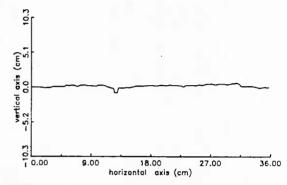
RMS = 0.264 cm
Max elev. diff. in prof. : 1.309

ARA 2-30 F
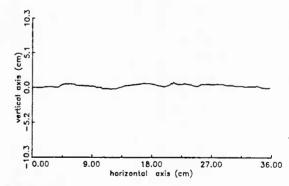
RMS = 0.274 cm
Max elev. diff. in prof. : 1.369

ARA 2-30 E
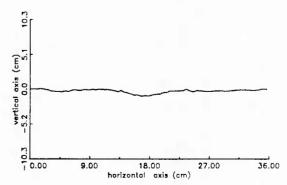
RMS = 0.223 cm
Max elev. diff. in prof. : 1.475

ARA 2-30 D
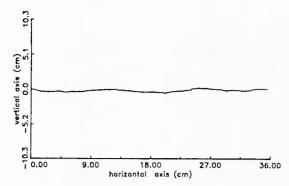
RMS = 0.221 cm
Max elev. diff. in prof. : 1.031

ARA 2-30 C
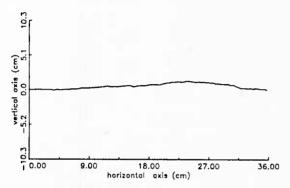
RMS = 0.265 cm
Max elev. diff. in prof. : 1.074

76

ARA 2-30 B
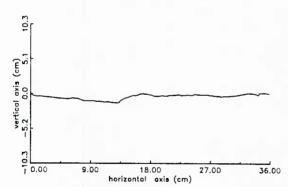
RMS = 0.182 cm
Max elev. diff. in prof. : 0.781

ARA 2-30 A
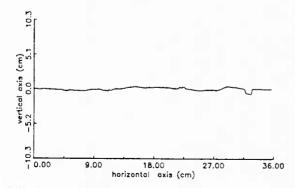
RMS = 0.404 cm
Max elev. diff. in prof. : 1.353

ARA 2-29 F
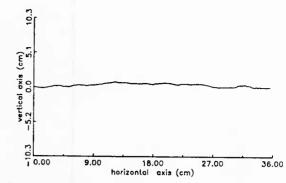
RMS = 0.389 cm
Max elev. diff. in prof. : 1.487

ARA 2-29 E
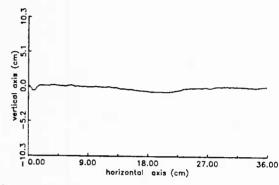
RMS = 0.209 cm
Max elev. diff. in prof. : 1.188

ARA 2-29 D
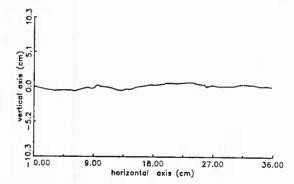
RMS = 0.248 cm
Max elev. diff. in prof. : 0.942

ARA 2-29 C
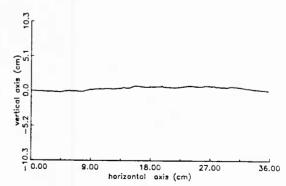
RMS = 0.281 cm
Max elev. diff. in prof. : 1.003

ARA 2-29 B
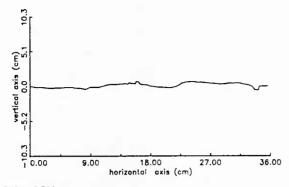
RMS = 0.360 cm
Max elev. diff. in prof. : 1.279

ARA 2-29 A
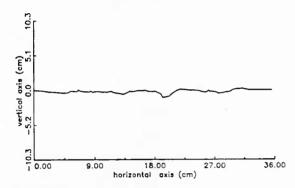
RMS = 0.291 cm
Max elev. diff. in prof. : 0.969

77

ARA 2-19 F
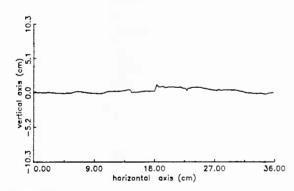
RMS = 0.322 cm
Max elev. diff. in prof. : 1.295

ARA 2-19 B

RMS = 0.267 cm
Max elev. diff. in prof. : 0.951

ARA 2-19 E

RMS = 0.234 cm
Max elev. diff. in prof. : 1.337

ARA 2-19 A
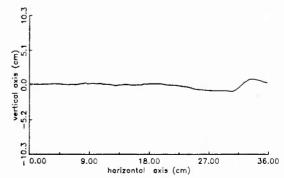
RMS = 0.215 cm
Max elev. diff. in prof. : 0.874

ARA 2-19 D

RMS = 0.327 cm
Max elev. diff. in prof. : 1.375

ARA 2-5 F
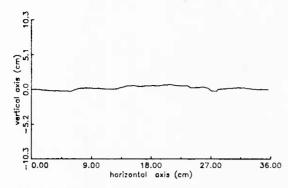
RMS = 0.130 cm
Max elev. diff. in prof. : 0.503

ARA 2-19 C

RMS = 0.211 cm
Max elev. diff. in prof. : 0.894

ARA 2-5 E
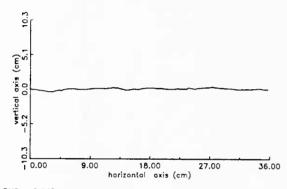
RMS = 0.416 cm
Max elev. diff. in prof. : 1.805

ARA 2-5 D
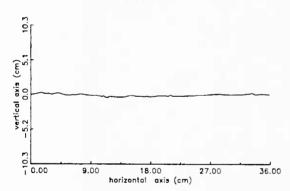
RMS = 0.282 cm
Max elev. diff. in prof. : 1.054

ARA 2-5 C
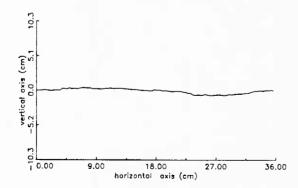
RMS = 0.143 cm
Max elev. diff. in prof. : 0.789

ARA 2-5 B
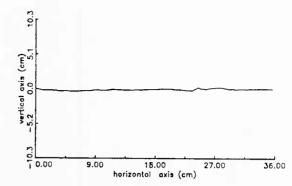
RMS = 0.178 cm
Max elev. diff. in prof. : 0.756

ARA 2-5 A
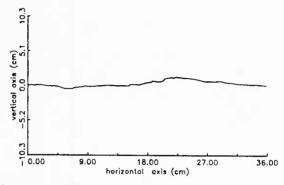
RMS = 0.335 cm
Max elev. diff. in prof. : 1.127

ARA 2-4 F
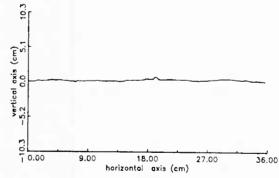
RMS = 0.147 cm
Max elev. diff. in prof. : 0.649

ARA 2-4 E
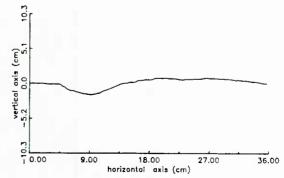
RMS = 0.451 cm
Max elev. diff. in prof. : 1.782

ARA 2-4 D
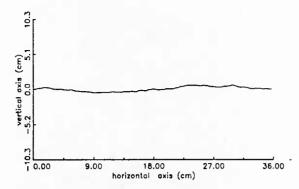
RMS = 0.137 cm
Max elev. diff. in prof. : 0.776

ARA 2-4 C
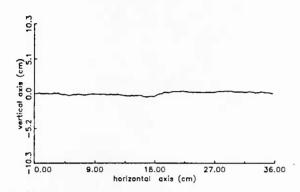
RMS = 0.724 cm
Max elev. diff. in prof. : 2.445

79

ARA 2-4 B
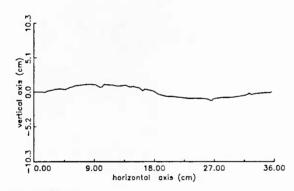
RMS = 0.340 cm
Max elev. diff. in prof. : 1.160

ARA 2-3 D

RMS = 0.318 cm
Max elev. diff. in prof. : 1.404

ARA 2-4 A
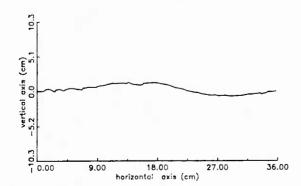
RMS = 0.228 cm
Max elev. diff. in prof. : 0.891

ARA 2-3 C

RMS = 0.642 cm
Max elev. diff. in prof. : 1.901

ARA 2-3 F
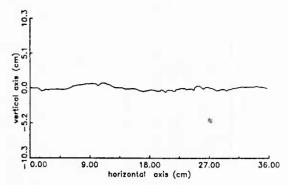
RMS = 0.728 cm
Max elev. diff. in prof. : 2.385

ARA 2-3 B

RMS = 0.627 cm
Max elev. diff. in prof. : 2.295

ARA 2-3 E
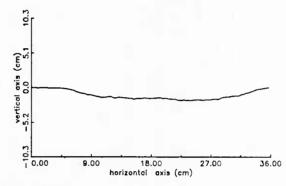
RMS = 0.646 cm
Max elev. diff. in prof. : 2.028

ARA 2-3 A
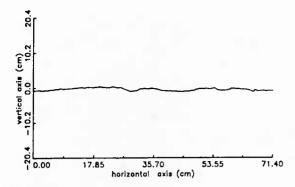
RMS = 0.552 cm
Max elev. diff. in prof. : 2.102

80

Appendix C2
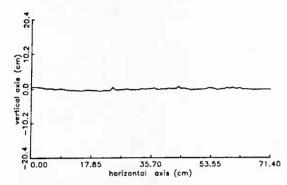
Bottom Roughness Height Data
for 71.4-cm Pathlengths

Relative sediment height versus pathlength for random orientations in 14 stereo photographs from 71.4-cm pathlengths. Profile 1-43* is the second cross-sectional line from stereo photograph #1-43.

ARA 1-10
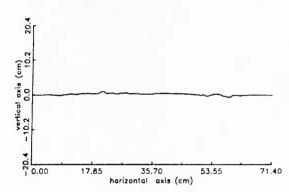
RMS = 0.391 cm
Max elev. diff. in prof. : 1.492

ARA 1-16
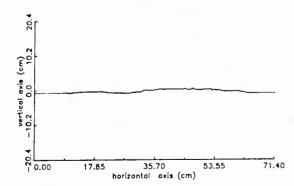
RMS = 0.268 cm
Max elev. diff. in prof. : 1.358

ARA 1-21
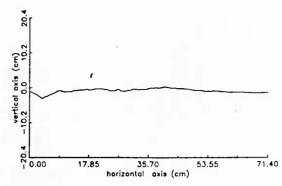
RMS = 0.276 cm
Max elev. diff. in prof. : 1.619

ARA 1-30
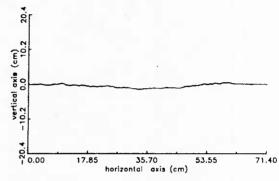
RMS = 0.432 cm
Max elev. diff. in prof. : 1.499

ARA 1-33
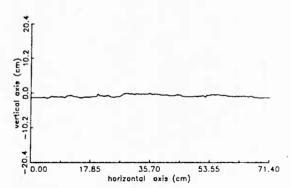
RMS = 0.650 cm
Max elev. diff. in prof. : 3.509

ARA 1-37
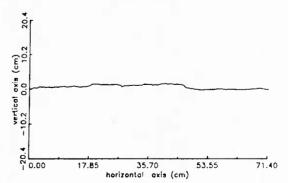
RMS = 0.532 cm
Max elev. diff. in prof. : 2.043

ARA 1-39
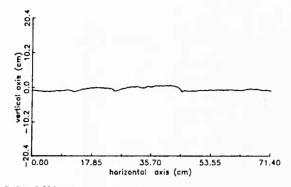
RMS = 0.368 cm
Max elev. diff. in prof. : 1.503

ARA 1-43
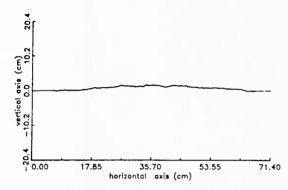
RMS = 0.585 cm
Max elev. diff. in prof. : 1.884

82

ARA 1-43•
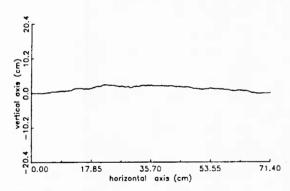
RMS = 0.506 cm
Max elev. diff. in prof. : 1.857

ARA 1-50

RMS = 0.548 cm
Max elev. diff. in prof. : 2.404

ARA 1-44
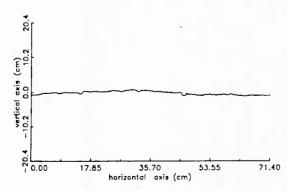
RMS = 0.574 cm
Max elev. diff. in prof. : 1.965

ARA 1-54

RMS = 0.188 cm
Max elev. diff. in prof. : 0.967

ARA 1-45
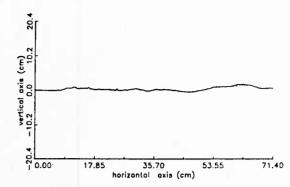
RMS = 0.792 cm
Max elev. diff. in prof. : 2.600

ARA 1-55
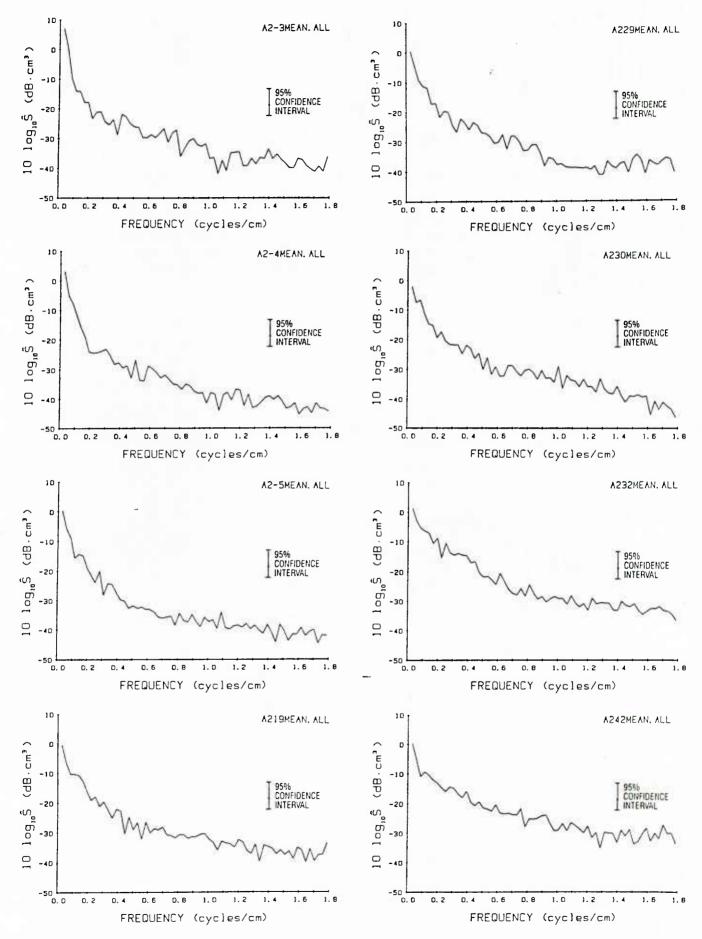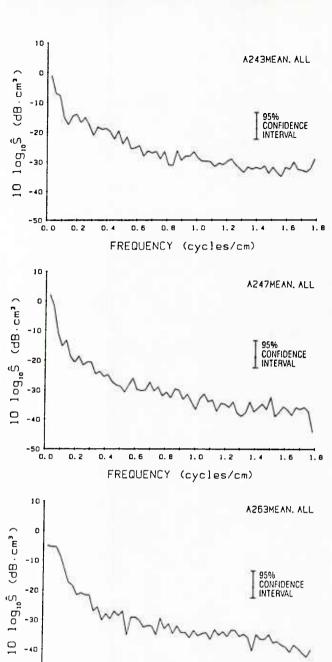
RMS = 0.295 cm
Max elev. diff. in prof. : 1.273

ARA 1-49

RMS = 0.512 cm
Max elev. diff. in prof. : 1.830

83
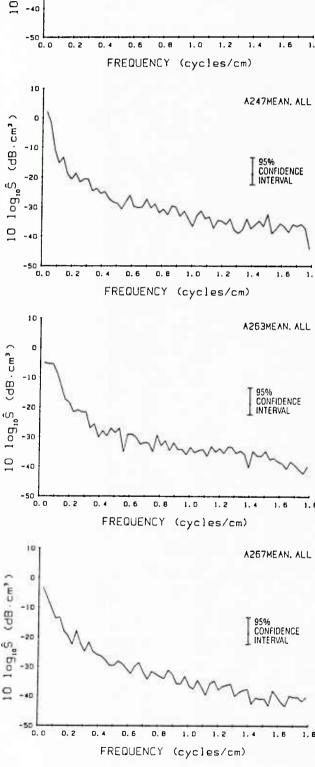
Appendix D1
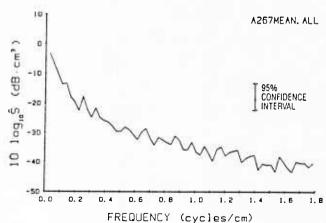
Roughness Power Spectra
for 35.56-cm Pathlengths
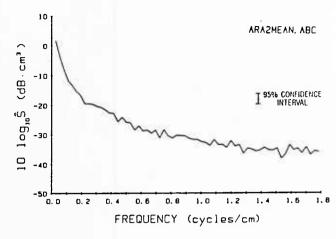
Periodograms depicting the average power spectral density functions for each of the 12 stereo photographs digitized at the 3-foot focal length (35.56-cm pathlength). Each plot is an average of all six cross-sectional lines (A-F), except for the last two periodograms: Each plot is an average of all 36 cross-sectional lines north-south (A-C) or east-west (D-F).

87
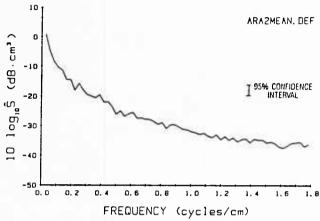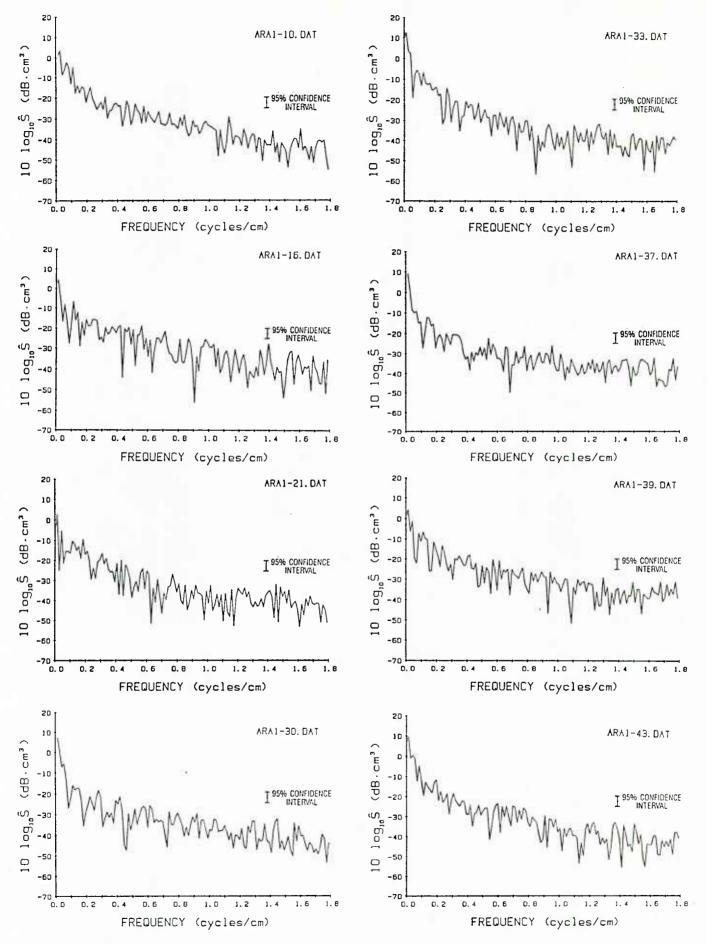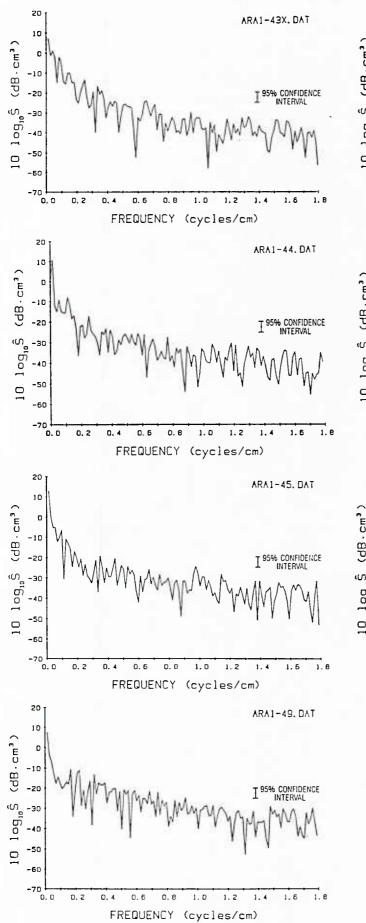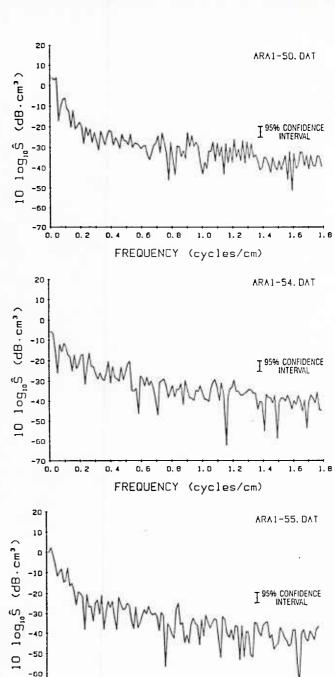
Appendix D2

Roughness Power Spectra
for 71.4-cm Pathlengths

Periodograms depicting the power spectral density functions for each of the 15 cross-sectional lines digitized at the 4-foot focal length (71.4-cm pathlength).

90

ARA1-43X.DAT

ARA1-50.DAT

ARA1-44.DAT

ARA1-54.DAT

ARA1-45.DAT

ARA1-55.DAT

ARA1-49.DAT

91

Distribution List

Asst Secretary of the Navy
(Research, Engineering & Systems)
Navy Department
Washington DC 20350-1000

Chief of Naval Operations
Navy Department (OP-02)
Washington DC 20350-2000

Chief of Naval Operations
Navy Department (OP-71)
Washington DC 20350-2000

Director
National Ocean Data Center
WSC1 Room 103
6001 Executive Blvd.
Attn: G. W. Withee
Rockville MD 20852

Chief of Naval Operations
Navy Department (OP-987)
Washington DC 20350-2000

Oceanographer of the Navy
Chief of Naval Operations
Attn: OP-096
U.S. Naval Observatory
34th & Mass Ave., NW
Washington DC 20390-1800

Commander
Naval Air Development Center
Warminster PA 18974-5000

Commanding Officer
Naval Coastal Systems Center
Panama City FL 32407-5000

Commander
Space & Naval Warfare Sys Com
Washington DC 20363-5100

Commanding Officer
Naval Environmental Prediction
Research Facility
Monterey CA 93943-5006

Commander
Naval Facilities Eng Command
Naval Facilities Eng Command Headquarters
200 Stovall St.
Alexandria VA 22332-2300

Commanding Officer
Naval Ocean R&D Activity
Attn: Code 100
Stennis Space Center MS 39529-5004

Commanding Officer
Naval Ocean R&D Activity
Attn: Code 125L (13)
Stennis Space Center MS 39529-5004

Commanding Officer
Naval Ocean R&D Activity
Attn: Code 125P (1)
Stennis Space Center MS 39529-5004

Commanding Officer
Naval Ocean R&D Activity
Attn: Code 105
Stennis Space Center MS 39529-5004

Commanding Officer
Naval Ocean R&D Activity
Attn: Code 115
Stennis Space Center MS 39529-5004

Commanding Officer
Naval Ocean R&D Activity
Attn: Code 200
Stennis Space Center MS 39529-5004

Commanding Officer
Naval Ocean R&D Activity
Attn: Code 300
Stennis Space Center MS 39529-5004

Commanding Officer
Naval Research Laboratory
Washington DC 20375

Commander
Naval Oceanography Command
Stennis Space Center MS 39529-5000

Commanding Officer
Fleet Numerical Oceanography Center
Monterey CA 93943-5005

Commanding Officer
Naval Oceanographic Office
Stennis Space Center MS 39522-5001

Commander
Naval Ocean Systems Center
San Diego CA 92152-5000

Commanding Officer
ONR Branch Office
Box 39
FPO New York NY 09510-0700

Commander
David W. Taylor Naval Research Center
Bethesda MD 20084-5000

Commander
Naval Surface Weapons Center
Dahlgren VA 22448-5000

Commanding Officer
Naval Underwater Systems Center
Newport RI 02841-5047

Superintendent
Naval Postgraduate School
Monterey CA 93943

Director of Navy Laboratories
Rm 1062, Crystal Plaza Bldg 5
Department of the Navy
Washington DC 20360

Officer in Charge
New London Laboratory
Naval Underwater Sys Cen Det
New London CT 06320

Director
Office of Naval Research
Attn: Code 10
800 N. Quincy St.
Arlington VA 22217-5000

Director
Woods Hole Oceanograhic Inst
P.O. Box 32
Woods Hole MA 02543

University of California
Scripps Institute of Oceanography
P.O. Box 6049
San Diego CA 92106

Officer in Charge
Naval Surface Weapons Center Det
White Oak Laboratory
10901 New Hampshire Ave.
Attn: Library
Silver Spring MD 20903-5000

Commanding Officer
Fleet Anti-Sub Warfare Training Center, Atlantic
Naval Station
Norfolk VA 23511-6495